Doctoral Thesis

Study on the gut coiling morphogenesis in *Xenopus* larvae

両生類アフリカツメガエル幼生腸管の巻きの形態形成の研究

Kanagawa University,

Graduate School of Science, Field of Biological Science, Doctoral Program

Ryuji Toyoizumi Laboratory

Student ID Number: 201870181

Kaoru Akinaga

神奈川大学大学院　理学研究科理学専攻生物科学領域　博士後期課程

豊泉　龍児　研究室

学籍番号：　201870181

秋永　薫

Index

Study on the gut coiling morphogenesis in *Xenopus* larvae
両生類アフリカツメガエル幼生腸管の巻きの形態形成の研究

豊泉龍児研究室　　秋永　薫　　(201870181)

脊椎動物の腸管は、消化吸収を担う消化管上皮構造と高度に組織化し蠕動運動を担う平滑筋による筋構造を有する。発生過程において腸管の消化管上皮がその面積を拡充する際には、腸管は伸長しつつかつ同時に固有のパターンで巻いて折りたたまれ、左右非対称な形態形成を行う。筆者は、高い透明性をもつアフリカツメガエル初期幼生を用いて、「幼若な腸管の形態形成にはその平滑筋の actomyosin 系の時空間的に制御された収縮活性が必要である」との作業仮説をもとに実験研究を行った。

平滑筋特異的 actin (SM-actin)の分布と配向を可視化するために、whole-mount のツメガエル幼生をサンプルとして抗-SM-actin 抗体による免疫染色を行った。その結果、ツメガエル初期幼生の腸管においてSM-actin の発現領域が発生段階依存的に拡大していくことを見出した。さらに、腸管の長軸(伸長方向)に直交する横断方向に腸管平滑筋がまずは配向し、次いで腸管の軸に沿った長軸方向に腸管平滑筋が配向することも発見した。更に、こうして生成された腸管平滑筋がつくる縦横の格子には、腸管の巻きの中心のみで異方性 (anisotropic)を示す捻じれが生じることも新たに見出した。actin と対をなす myosin の配向を、SM-actin と同様に免疫染色により可視化した。活性化した状態の myosin を検出する抗リン酸化 myosin 軽鎖抗体を用いた免疫染色により、ツメガエル正常胚の myosin については、SM-actin の場合と同様に腸管において横断方向にリン酸化 myosin 陽性細胞が配向し、次いで腸管の軸に沿った長軸方向にリン酸化 myosin 陽性細胞が配向した。リン酸化myosin 陽性細胞の縦横の格子にも、抗-SM-actin 抗体で染めた場合と同様に腸管の巻きの形態形成の中心のみで異方性を示す捻じれが生じていた。2 つの抗体で染まった細胞は、SM-actin が主要な平滑筋マーカーであることから、共に腸管平滑筋細胞であると思われる。これら二つの相互に符合する発見は、捻じれによる機械的な力が腸管の左右非対称な巻きの形態形成に関与していることを示唆している。次に、myosin II ATPase の阻害を通じて actomyosin の相互作用を阻害する Blebbistatin をツメガエル後期胚から初期幼生期にかけて投与した。その結果、腸管は巻きの形態形成の程度が弱まるか、左右相称に背腹方向のみに蛇行し螺旋状には巻かなくなった。

上述の whole-mount の実験系では Blebbistatin 投与による他の組織への副次的な影響で腸管の形態形成が阻害されたにすぎないとの虞があった。そこで筆者は *in vitro* で腸管の巻きの形態形成を評価するモデル培養系の作出を行い、これに成功した。それに先立ち、最初にいわゆる半胚の作成により、腸管の形態形成への影響の評価を行った。神経胚期から尾芽胚期にかけてのツメガエル胚は胴部を二つに切断しても数日間は生存する高度な傷口修復能力を備えている。この性質を活かして、以下の 3 つのパターンで切断した半胚を短期間培養し、腸管形態形成を評価した。前頭部を切断しかつ心臓を残した胚では、98.5%の胚で腸管は正常に st.46 の巻き方で巻いた。頭部とともに心臓も除外するように前胸部も切断した胚でも 21.1%は途中まで正常に巻いた。頭部と尾部の双方を切断した胚では、一部の個体で途中まで腸管が巻いた。これらの結果から腸管の巻きの形態形成はある程度自律的に進行することが分かった。

以上のように、筆者が新規に開発した腸管原基の外植体の培養結果からは、ツメガエル幼生の腸管の巻きがかなりの程度、他の器官との相互作用無しに進行することが明らかとなった。そこで、次に単離腸管だけで巻く器官培養の系を作出することを試みた。腸管が巻き出す直前の発生段階である st. 41 の

ツメガエル胚から腸管を単離し、CO_2非依存培地を用いて通常の気相下で培養した。その結果、外植体に巻きの形態形成を誘導することに成功した。このことから、*in vitro* で単離腸管が組織自律的に巻くことが分かったといえる。この筆者独自の腸管外植体培養系において薬剤投与実験を行った。actin 重合阻害剤 CK-666、myosin light chain kinase 阻害剤 ML-9、calmodulin アンタゴニスト W-7 の 3 薬剤をそれぞれ投与することで actomyosin の収縮を阻害し、外植体への影響を評価した。いずれの薬剤投与群でも、巻きの形態形成を行う外植体の頻度が対照群に較べて有意に低下した(いずれも $p<0.01$)。また、細胞骨格の集積に関与する ROCK に特異的な阻害剤 Y-27632 を投与した単離腸管は全く巻かなかった。重要なことは、whole-mount の実験でも投与した Blebbistatin を単離腸管に浸漬処理すると、単離腸管の巻きの形態形成は阻害された。

以上の器官培養系の実験結果から腸管の巻きの形態形成において actomyosin の関与は非常に濃厚になったと判断したので、筆者は次に腸管の巻きを司る細胞間シグナル伝達経路を探索することにした。筆者はここでツメガエル後期胚-幼生期の腸管において発現している分泌因子 Wnt のシグナル伝達経路に注目した。Wnt リガンドの分泌を阻害する阻害剤 Wnt C-59 を投与したところ、単離腸管が巻く頻度が低下した。また、whole-mount で Wnt シグナルの細胞内経路のうち古典経路のみを阻害する Cardionogen-1 を投与した所、ツメガエル幼生の腸管の巻きは弱まるか、停止した。これらの結果から、腸管の巻きの形態形成に Wnt シグナル伝達経路が関与していることが示唆された。

本研究は、(1) *in vivo* での SM-actin やリン酸化 myosin を発現する腸管平滑筋の分布の観察、(2) 胴体部半胚での腸管の形態形成の評価、(3) 阻害剤投与を組み合わせた腸管外植体の *in vitro* 培養系...の 3 つの階層の実験を有機的に組み合わせてツメガエル初期幼生の腸管の形態形成の機構を解析した。得られた一連の実験結果から、腸管が巻き始める初期幼生期のツメガエル腸管では actomyosin の相互作用依存的に腸管が折りたたまれて巻くことが判った。腸管平滑筋が時空間依存的に格子状に配向し、そして捻れることが、腸管の折りたたみを駆動することも判った。本研究の一連の実験結果からは、巻きの形態形成はかなりの程度腸管自律的に行われることも明らかとなった。初期幼生期での actomyosin の相互作用により生じる収縮力が、筋肉性器官である腸管の正常な巻きのパターンの確立に不可欠であることが本研究により明らかとなった。

In vertebrates, gut coiling proceeds left-right asymmetrically during expansion of the gastrointestinal tract with highly organized muscular structures facilitating peristalsis. In this report, we explored the mechanisms of larval gut coiling morphogenesis relevant to its nascent smooth muscle cells using highly transparent Xenopus early larvae. First, to visualize the dynamics of intestinal smooth muscle cells, whole-mount specimens were immunostained with anti-smooth muscle-specific actin (SM-actin) antibody. We found that the nascent gut of Xenopus early larvae gradually expands the SM-actin-positive region in a stage-dependent manner. Transverse orientation of smooth muscle cells was first established, and next, the cellular longitudinal orientation along the gut axis was followed to make a meshwork of the contractile cells. Finally, anisotropic torsion by the smooth muscle cells was generated in the center of gut coiling, suggesting that twisting force might be involved in the late phase of coiling morphogenesis of the gut. Administration of S-(–)-Blebbistatin to attenuate the actomyosin contraction in vivo resulted in cancellation of coiling of the gut. Development of decapitation embryos, trunk 'torso' explants, and gut-only explants revealed that initial coiling of the gut proceeds without interactions with the other parts of

the body including the central nervous system. We newly developed an in vitro model to assess the gut coiling morphogenesis, indicating that coiling pattern of the nascent Xenopus gut is partially gut-autonomous. Using this gut explant culture technique, inhibition of actomyosin contraction was performed by administrating either actin polymerization inhibitor, myosin light chain kinase inhibitor, or calmodulin antagonist. All of these reagents decreased the extent of gut coiling morphogenesis in vitro. Taken together, these results suggest that the contraction force generated by actomyosin-rich intestinal smooth muscle cells during larval stages is essential for the normal coiling morphogenesis of this muscular tubular organ.

1. Abstract

In vertebrates, gut coiling proceeds left-right asymmetrically during expansion of the gastrointestinal tract with highly organized muscular structures facilitating peristalsis. In this report, we explored the mechanisms of larval gut coiling morphogenesis relevant to its nascent smooth muscle cells using highly transparent Xenopus early larvae. First, to visualize the dynamics of intestinal smooth muscle cells, whole-mount specimens were immunostained with anti-smooth muscle-specific actin (SM-actin) antibody. We found that the nascent gut of Xenopus early larvae gradually expands the SM-actin-positive region in a stage-dependent manner. Transverse orientation of smooth muscle cells was first established, and next, the cellular longitudinal orientation along the gut axis was followed to make a meshwork of the contractile cells. Finally, anisotropic torsion by the smooth muscle cells was generated in the center of gut coiling, suggesting that twisting force might be involved in the late phase of coiling morphogenesis of the gut. Administration of S-(–)-Blebbistatin to attenuate the actomyosin contraction in vivo resulted in cancellation of coiling of the gut. Development of decapitation embryos, trunk 'torso' explants, and gut-only explants revealed that initial coiling of the gut proceeds without interactions with the other parts of the body including the central nervous system. We newly developed an in vitro model to assess the gut coiling morphogenesis, indicating that coiling pattern of the nascent Xenopus gut is partially gut-autonomous. Using this gut explant culture technique, inhibition of actomyosin contraction was performed by administrating either actin polymerization inhibitor, myosin light chain kinase inhibitor, or calmodulin antagonist. All of these reagents decreased the extent of gut coiling morphogenesis in vitro. Taken together, these results suggest that the contraction force generated by actomyosin-rich intestinal smooth muscle cells during larval stages is essential for the normal coiling morphogenesis of this muscular tubular organ.

2. Introduction

In this thesis, I explored the causative factors that regulate and guide the coiling morphogenesis of the nascent gut. In vertebrates, to expand the area of the gastrointestinal tract supporting the digestion of food and the absorption of nutrients, gut coiling morphogenesis occurs in a species-specific and developmental stage-dependent manner (Hamburger and Hamilton, 1951; Nieuwkoop and Faber 1967). Via orchestrated coiling morphogenesis, elongation of the muscular gut tube is systematically compacted in the abdominal cavity, and animals regulate the length of the gut tube according to feeding habits (Dasgupta, 2004; Koundal et al., 2012).

The morphogenesis of vertebrate digestive systems might be controlled by the developmental schedule of smooth muscle differentiation. In vertebrates, the long intestine is packaged by gut coiling in an anticlockwise manner when viewed from the ventral side (Nieuwkoop and Faber 1967). Intestinal primordium forms a tube that loops and then coils. Intestinal peristaltic movement requires fine control of smooth muscle precursor migration, proliferation, and differentiation. The intestinal epithelium, derived from endoderm, forms a tubular structure, and mesenchymal cells originating from the splanchnic mesoderm layer of the lateral plate mesoderm (LPM) migrate toward the epithelial tube and surround it. During this event in zebrafish, mutual pushing by the LPMs and the

resultant crawling movement of the frontal edge of the LPM determine the orientation of intestinal looping (Horne-Badovinac et al., 2003). Laminin, one of the major components constituting extracellular matrix, is a key factor for this crawling movement (Hochgreb-Hägele et al., 2013). In chick and mouse embryos, intestinal looping is controlled by the mesentery; the looping direction of the intestine is decided by differential growth and size between left and right mesodermal epithelia of the dorsal mesentery, and left-specific *pitx2* expression is a key regulator of this mechanism (Davis et al., 2008). BMP signaling controls this event by influencing *pitx2* expression level at the dorsal mesentery, at least in chick embryos (Nerurkar et al., 2017). Cytoskeletal components such as myosin also contribute to establish intestinal left-right asymmetry via ciliary flow in vertebrate embryos (Hozumi et al., 2006; Tingler et al., 2018).

In the present work, I first observed the orchestrated dynamics of nascent gut smooth muscle cells during the coiling morphogenesis, using early stage larvae of the African clawed frog (*Xenopus laevis*), an amphibian organism widely employed as a vertebrate model. *X. laevis* larvae have a translucent epidermis, particularly in the melanophore-free ventral thoracic and abdominal regions, which makes it easy to non-invasively observe organ morphogenesis of the visceral organs. I speculate that prior to the actual contraction of gut smooth muscle cells, cellular coordination of myoblasts mediated by mutual adhesion, orientation, and elongation toward a certain direction is needed to generate the directional contraction force of the nascent gut tube during the appropriate developmental stage. Thus, using *Xenopus* early larvae, I examined stage-depended distribution and its transition of intestinal smooth muscle cells by immunohistochemistry using antibodies for smooth muscle specific SM-actin and phosphorylated myosin. In results, I first obtained the results of highly orchestrated collaborative migration and orientation of nascent smooth muscle cells and its meshwork formation.

I next explore the mechanisms of gut coiling by developing unique gut explant culture techniques to know the molecular cue that guide the gut coiling morphogenesis. I predict that the mechanical force resulting from the contraction and related activities of gut smooth muscle cells is likely involved in gut coiling morphogenesis. The actomyosin system is directly responsible for muscular contraction. Gut smooth muscle cells also possess smooth muscle-specific actin and, even though not yet fully identified, some myosin isoforms (Georgijevic et al., 2007, Barillot et al., 2008). I employed an explant culture approach in combination with the administration of the reagents to investigate the effects of experimental treatments during pivotal early larval stages of gut coiling organogenesis. Few studies on actin-myosin interactions have been conducted from the viewpoint of the organogenesis of differentiating muscular structures (Marston and Goldstein, 2006). However, embryos are known to undergo tissue contraction and muscular morphogenesis involving immature and continuously differentiating myoblasts (Ma and Adelstein, 2012). Thus, embryonic organogenesis based on actual contraction of contractile immature smooth muscle cells is fascinating, so understanding this process has been pursued for a long time.

In this thesis, I examined whether the intestinal tube loops and then coils via mechanical contractile force generated by actin-myosin interactions. To inhibit myosin ATPase activity for contraction, I

used Blebbistatin, a well-characterized inhibitor of non-muscle myosin II ATPase (Kovács et al., 2004; Kampourakis et al., 2018). Blebbistatin inhibits the release of inorganic phosphate, which impedes myosin II function (Kovács et al., 2004). Myosin II is known to be expressed in the *Xenopus* intestine (Session et al., 2016). In the present study, after administering this reagent during the developmental stage immediately preceding the onset of coiling morphogenesis in the gut, its effects on morphogenesis of the gut were observed in combination with immunohistochemistry using antibodies recognizing the smooth muscle-specific muscle marker SM-actin. The results showed that attenuation and/or retardation of coiling morphogenesis of the larval intestine, leading to cancellation of left-right asymmetry without coiling, was induced following administration of Blebbistatin.

Finally, explant culture of amputated trunk explants (containing gut domains) and isolated gut rudiments was performed, and the results revealed that the explant culture technique could identify tissues essential for minimal coiling morphogenesis. Additionally, CM-666, Blebbistain, ML-9, and W-7, four reagents that block actomyosin contraction, were applied to the explants, and changes in the manner of coiling morphogenesis were assessed (Tanaka and Hidaka 1980, Itoh and Hidaka 1984, Asano 1990, Wang et al., 2007, Nolen et al., 2009, Várnai et al., 2009, Park et al., 2010, Hetrik et al., 2013, Ilatovskaya et al., 2013).

Based on the presented results, I discuss the possible roles of smooth muscle cells and its contractile activities in coiling morphogenesis of the *Xenopus* larval gut.

3. Materials and Methods

Experimental animals and preparation of embryos

Throughout all experiments, late stage embryos or early larvae of *Xenopus laevis* (family Pipidae, order Anura) were employed. A couple of adult frogs were injected with gonadotropin (females 500 units, males 300 units), and fertilized eggs were obtained by natural spawning. After exfoliating and removing the jelly coat by thioglycolic acid immersion (pH 8.6), early embryos were incubated in 10% Steinberg solution (artificial fresh water for frog embryos) at 16-24°C until the appropriate developmental stage was reached. Determination of the developmental stage was performed in accordance with the normal stage table by Nieuwkoop and Faber (1967).

Immunohistochemistry of wholemount specimen and intestine samples

Using immunohistochemistry, the localization and distribution of actomyosin were examined. Primary antibodies were used as follows: anti-alpha-Smooth Muscle actin (SM-actin) mouse monoclonal antibody (Sigma-Aldrich Co., St. Louis, Missouri, USA) for smooth muscle actin; anti-phospho-Myosin Light Chain 2 (Ser19) rabbit polyclonal antibody (Cell signaling Technology, USA) for phosphorylated myosin light chain; 12/101 mouse monoclonal antibody known to recognize skeletal muscle (provided by the Developmental Studies Hybridoma Bank [DSHB]). As a secondary antibody, Alexa Fluor 488-conjugated AffiniPure Fab Fragment goat anti-Mouse IgG H+L (Thermo Fisher Scientific Co., Waltham, Massachusetts, USA) and Goat anti-Rabbit IgG (H+L) Secondary Antibody, DyLight 594 (Thermo Fisher Scientific Co., Waltham, Massachusetts, USA), were used. For control experiments, specimens without treating with first antibodies targeting anti-SM-actin or anti-phosphorylated myosin were prepared for observations.

Stage 38-46 larvae were fixed with 4% paraformaldehyde / phosphate-buffered saline (PBS(–), pH 7.2-7.4, without Mg^{2+} and Ca^{2+} ions) for 1.5-2 h, and then dipped in 100% methanol and stirred for 5 min twice. Fixed samples were stirred for 5 min in a series of diluted methanol solutions (75%, 50%, and 25% methanol) in PBS(–) containing 0.1% (v/v) Tween-20 detergent (PBST). Samples were immersed in PBST by stirring for 5 min twice, and then immersed in 400 µl of 3% Blocking reagent in PBST for 1 h at room temperature. The solution was exchanged with 150 µl of primary antibody solution prepared with 3% Blocking reagent in PBST, and samples were incubated at 4°C overnight or for 2 days. Samples were washed five times with PBST for 20 min, and then immersed in 400 µl of 3% Blocking reagent in PBST for 1 h at room temperature. The solution was then exchanged with 150 µl of secondary antibody solution prepared with Blocking reagent in PBST, and samples were incubated overnight at 4°C. Finally, samples were washed five times with PBST for 20 min at room temperature, and then washed five times with PBS for 5 min.

Counterstaining of parts of the specimens was performed using CellMask® (Thermo Fisher Scientific Co.) to visualize the plasma membrane. CellMask was diluted with PBS(–) at a concentration of 5 µg/ml and, after removing the abdominal body wall muscle with forceps, specimens immunostained with SM-actin antibody were immersed in CellMask diluent for 15 min with stirring at 60 rpm. After washing twice for 5 min with stirring at 60 rpm, samples were observed

using an SZX16 fluorescence stereoscopic microscope (Olympus Co.), an IX-73 fluorescence-inverted microscope (Olympus Co.), or an LSM700 confocal laser-scanning microscope (Carl Zeiss AG, Oberkochen, Deutschland).

Administration of Blebbistatin to whole-mount specimens

Treatment of the wholemount specimens with (±)-Blebbistatin [1,2,3,3a-tetrahydro-3a-hydroxy-6-methyl-1-phenyl-4H-pyrrolo[2,3-b]quinolin-4-one); molecular formula $C_{18}H_{16}N_2O_2$; molecular weight 292.3] was performed. Blebbistatin is a potent non-muscle myosin II ATPase inhibitor (Nie et al., 2015). Stage 38-39 late-tailbud embryos were immersed in 0.05 μM or 0.1 μM (±)-Blebbistatin / 0.1% dimethylsulfoxide (DMSO) / 10% Steinberg solution in an organ culture dish, and dishes were gently stirred at 60 rpm in a shaker under humid conditions at 24°C. As control experiments, siblings were immersed in 0.1% DMSO / 10% Steinberg solution without reagent under the same conditions. After 6 h, both experimental and control siblings were washed with 10% Steinberg solution, incubated with the same 10% Steinberg solution in wells of 24-well multi-well plates at a density of one embryo per well, and cultured to reach the appropriate stage. When control siblings reached larval stage 46, both experimental and control groups were observed using an SZX16 fluorescence stereoscopic microscope (Olympus Co., Shinjuku-ku, Tokyo, Japan), and the shapes of intestinal samples were photographed and scored. Movies of several larvae were recorded.

Treatment with optical isomers of Blebbistatin

Blebbistatin occurs in two optical isomers: R-(+)-Blebbistatin (inactive form) and S-(–)-Blebbistatin (active form) (Kovács et al., 2004). Stage 38-39 late-tailbud embryos were immersed in 0.05 μM or 0.1 μM R-(+)-Blebbistatin / 0.1% DMSO / 10% Steinberg solution as described above, or 0.05 μM or 0.1 μM S-(–)-Blebbistatin was administered. In part of the experiments, Stage 43-44 early larvae during the coiling process also immersed in 0.1 μM S-(–)-Blebbistatin solution for 6 hr. Sibling embryos were used as controls as described above.

Behavioral observation

For embryos subjected to (±)-Blebbistatin treatment, at 6 h after beginning the treatment, mechanical stimulation was performed by touching embryos with a hair-loop instrument. During this process, the behavior of embryos was recorded in movies.

Amputation and culture of partial embryos and explants

Xenopus tailbud embryos at stage 32-33 were anesthetized with 0.1% phenoxyethanol, and the head region of each embryo was amputated with microscissors by holding the embryo with forceps. The amputated embryos were cultured to stage 46 in 10% Steinberg's solution containing penicillin-streptomycin at 16°C. When untreated control siblings reached stage 46, gut coiling was scored for both experimental and control groups. Three patterns of amputation were performed: (i) removal of the frontal head region, leaving both the heart and tail intact; (ii) removal of both the head region and

the heart, leaving the tail intact; and (iii) removal of the head region, the heart, and the tail (Fig. 6A).

Isolation of immature gut tissue before coiling and explant culture to estimate the extent of coiling

Gut primordium tissue before substantial looping was isolated from stage 41 early *Xenopus* larvae using forceps and microscissors. The isolated gut explants were cultured at 24°C in 70% diluted CO_2-independent medium® (Thermo Fisher Scientific Co.) containing penicillin-streptomycin (Fig. 7A). In case of (±)-Blebbistain treatment to the gut explants *in vitro*, the CO_2-independent medium was not used because (±)-Blebbistatin seemingly react with the CO_2-independent medium and resultant precipitation was significant. Thus, alternatively, HBSS with 10mM HEPES without Phenol Red (STEMCELL Technologies, Canada) was used as the medium only for the (±)-Blebbistatin treatment. After 1 day of culture, the morphology of gut explants was classified into three patterns: looping (successful looping), U-shaped, and no looping (straight).

In the next step, each of the three reagents that can decrease the force of actomyosin contraction was administered separately during culture. As a control experiment, gut explants from sibling embryos were cultured in the same medium containing 0.1% DMSO. Details of the three reagents used were as follows:

(1) CK-666 (2-fluoro-N-[2-(2-methyl-1H-indol-3-yl)ethyl]benzamide), an inhibitor of F-actin formation (an actin polymerization inhibitor that disrupts the formation of the Arp2/3 molecular complex); molecular formula $C_{18}H_{17}FN_2O$, MW = 296.34 (Nolen et al., 2009, Hetrik et al., 2013, Ilatovskaya et al., 2013).

(2) ML-9 (1-(5-chloronaphthalenesulfonyl)homopiperazine hydrochloride), an inhibitor of myosin light chain kinase (MLCK); molecular formula $C_{15}H_{17}ClN_2O_2S.HCl$, MW = 361.29 (Wang et al., 2007, Várnai et al., 2009, Park et al., 2010).

(3) W-7 (N-(6-aminohexyl)-5-chloro-1-naphthalenesulfonamide hydrochloride), an inhibitor of calmodulin, a cytoplasmic Ca^{2+}-binding protein that inhibits the action of MLCK; molecular formula $C_{16}H_{21}ClN_2O_2S{\cdot}HCl$, MW = 377.33 (Tanaka and Hidaka 1980, Itoh and Hidaka 1984, Asano 1990).

(4) Y-27632 ((R)-(+)-trans-N-(4-Pyridyl)-4-(1-aminoethyl)-cyclohexanecarboxamide hydrochloride), an inhibitor of ROCK (Rho-associated protein kinase); molecular formula $C_{14}H_{21}N_3O{\cdot}2HCl$, MW=320.3 (Narumiya et al., 2000)

Titration for optimal concentration of the reagents

Based on the manufacturer's information and survival ratio, titration of the reagents used here was performed. Titer of (±)-Blebbistatin was examined in the range of 0.5–10 μM (0.5, 1, 5, 10 μM), and 0.5 or 1.0 μM was found to be optimal. CK-666, ML-9, Y-27632, and W-7 was examined in the range of 5–50 μM (5, 25, 50 μM), 5–75 μM (5, 10, 25, 50, 75 μM), 10–50 μM (10, 50 μM), and 10–100 μM (10, 50, 100 μM), respectively, and I choose the concentration of 50 μM (CK-666), 50 μM (ML-9), 50 μM (Y-27632) and 10 μM (W-7) to administer the reagents, respectively.

Statistical test

Statistical analysis of the extent of coiling morphogenesis in the experimental groups compared with the sibling explant control groups was performed using the 2X2 contingency table test (successful looping vs. U-shaped and/or abrogation of looping) at the 1% significance level.

4. Results

Stage-dependent expansion of the SM-actin-expressing domain and coordinate organization of smooth muscle cells during gut coiling morphogenesis

We examined stage-dependent expression of SM-actin during coiling morphogenesis of the gut by immunohistochemistry using anti-SM-actin monoclonal antibody, which recognizes SM-actin.

Immunostaining revealed gradual, stage-dependent changes in the regionality of the SM-actin-positive area (Fig. 1). At stage 42, most of the anterior gut tissue adjacent to the ventral pancreas expressed SM-actin, while the posterior gut did not yield a signal (Fig. 1A–A'). At stage 43, a strong SM-actin-positive domain was observed in the narrow duodenum region of the gut in all samples (Fig. 1B–B'). At stage 44, the SM-actin-positive area was expanded relative to that at stage 43, and the adjacent looping region also expressed SM-actin (Fig. 1C–C'). At stage 45, SM-actin was not fully expressed along the entire gut; rather, large parts of the gut expressed SM-actin (Fig. 1D–D'). At stage 46, SM-actin was expressed in the entire gut, which exhibited anticlockwise coiling (Fig. 1E–E').

Stage-dependent organization of SM-actin-positive cells elucidated by CLSM

Next, confocal laser-scanning microscopy (CLSM) was performed to generate 3-dimensional stacking images of the SM-actin-positive cells. To visualize the fine localization of SM-actin following stage-dependent expansion of the expression area, we observed whole-mount samples of stage 41–46 larvae by CLSM after immunostaining using anti-SM-actin antibody. In stage 41–42 early larvae, signals were weak and SM-actin-positive cells had not yet been organized (Fig. 2A–B). In stage 43 larvae, transverse orientation of the smooth muscle cells was first aligned along the region of the duodenum adjacent to the ventral pancreas (Fig. 2C, K). Patchy distribution of SM-actin was observed at the posterior-ventral stout region of the gut (Fig. 2D). However, the longitudinal cell orientation along the gut had not yet been organized. In stage 44 larvae, both transverse smooth muscle cells and longitudinal ones were observed in the duodenum and in the coiling center of the ventral left gut (Fig. 2E–F, K). These results indicate that that the organization of SM-actin-positive cells was first significant in the transverse direction perpendicular to the longitudinal axis of the gut, and longitudinal cells crossing over the transverse cells were subsequently observed in the expression domain (Fig. 2C–F, K). In other words, orientations of SM-actin-positive cells were coordinately formed first in the transverse direction of the intestinal axis and then in the longitudinal direction.

In addition, the CLSM results showed that anisotropic twisting of the cellular meshwork by SM-actin-positive cells was only observed in the core center during coiling morphogenesis in stage 45–46 samples (for stage 45 larvae, n = 6/10; for stage 46 larvae, n = 5/5; Fig. 2G–K). In other parts of the coiling gut, longitudinal cells along the length of the gut and transverse ones formed an orthogonal meshwork on the surface of the gut by stage 46. The results of immunostaining of SM-actin suggest that stage-dependent changes in SM-actin distribution and anisotropic twisting of cellular meshwork at the coiling center are essential for normal coiling morphogenesis.

Stage-dependent and sequential organization of the orthogonal lattice-like structure composed by the

phosphorylated myosin-positive cells.

To know the distribution of phosphorylated myosin in the nascent gut during the coiling morphogenesis, immunostaining with anti-phosphorylated myosin antibody coupled with fluorescent stereomicroscopy or CSLM observations was performed. Phosphorylated myosin light chain was uniformly distributed in low power magnification, which is in contrast with SM-actin distributions. Using CSLM, detailed observations of stage 41–46 early larvae were performed. During stage 41–42, no alignment of filamentous structure was recognized. In stage 43 larvae, transverse organization of filamentous positive cells was first recognized in the duodenum domain, which is coincidental with the organization of SM-actin-positive smooth muscle cells (Fig. 3A–C). After that, in stage 44 larvae, lattice-like structure of orthogonal meshwork of the filamentous cells was recognized in the frontal regions of the gut (duodenum and neighboring coiling region; Fig. 3D-F). In stage 45 larvae, torsion of such lattice-like structure was first observed in the central region of the coiling gut along the longitudinal axis. In stage 46 larvae, such torsion was fully established and significant in the center of the coiling gut (Fig. 3G–I). Taken together, we can say that sequential organization of the filamentous, phosphorylated myosin-positive cells undergoes in the similar manner of that of SM-actin, which implies that gut smooth muscle cells migrate, orient and contract to squeeze the nascent stout gut to coil by their anisotropic contractile force and thus are packaged in the limited abdominal space.

Administration of Blebbistatin to the wholemount specimen prevents gut coiling

Late stage embryos were immersed in artificial fresh water (10% Steinberg's solution) containing (±)-Blebbistatin, a well-characterized inhibitor of non-muscle myosin II ATPase. After Blebbistatin treatment, the early larval gut displayed attenuated/retarded gut coiling (n = 45/45 for 0.05 μM, n = 51/51 for 0.1 μM; Fig. 4B', C'). In particular, a substantial proportion of treated larvae displayed abrogated left-right asymmetric looping; there was a clear nullification of the left-right asymmetry of this normally asymmetric organ (n = 18/45 for 0.05 μM, n = 22/51 for 0.1 μM; Fig. 4C', Table 1). Retardation and/or hypoplasia of heart development was frequently observed after the treatment. Part of the stage 43–44 larvae during the coiling process were immersed in 0.1 μM S-(–)-Blebbistatin solution for 6 hr (Fig. 4D-D'). Control siblings underwent normal coiling and reached to stage 46 in one day, whereas treated larvae promptly arrested the coiling and keep the same extent of coiling at the onset of immersion stage for 1 day or more (n=23/23; Fig. 4D'). In several cases of the treated larvae, drift of the spiral plane was also observed (n=8/23). Sudden death of the treated larvae was frequently observed within a couple of days.

To examine the effects of (±)-Blebbistatin on the swimming behavior of early larvae, treated larvae were stimulated with a hair-loop instrument immediately after the treatment. In experimental larvae, all individuals ceased to respond to the touch stimulus (n = 4/4 for 0.05 μM, n = 4/4 for 0.1 μM), whereas untreated sibling larvae rapidly escaped from the touch stimulus. Based on these observations, we concluded that (±)-Blebbistatin did indeed inhibit the function of *Xenopus* myosin II.

Immersion experiments described above were performed mainly using (±)-Blebbistatin, a racemate composed of both R-(+)-Blebbistatin and S-(–)-Blebbistatin. To determine which isomer induces gut coiling disorder, we administered each component of the racemate to late stage embryos, and only S-(–)-Blebbistatin was found to induce gut looping disorder (n = 19/19 for 0.05 μM, n = 29/29 for 0.1 μM; Fig. 5C). By contrast, R-(+)-Blebbistatin had no effect on gut coiling morphogenesis when administered at the same concentrations (Fig. 5B). These results clearly demonstrate that only S-(–)-Blebbistatin, considered an active form of Blebbistatin, inhibits *Xenopus* myosin II function.

Next, using SM-actin antibody, which recognizes intestinal smooth muscle cells, we investigated the extent of differentiation of smooth muscles in the coiling gut after (±)-Blebbistatin treatment. The results showed that Blebbistatin frequently disordered the normal orientation of SM-actin-positive cells on the gut surface (n = 10/12 after 0.05 μM treatment, n = 11/12 after 0.1 μM treatment; Fig. 6A'). For comparison, we also performed immunostaining using 12/101 antibody, which recognizes skeletal muscle. Normal pattern of myotomes in the trunk and tail regions were not affected by Blebbistatin treatment (Fig. 6B–B'). In conclusion, immunostaining of SM-actin filaments following Blebbistatin treatment indicated that proper organization of the intestinal smooth muscles is likely needed for normal coiling morphogenesis.

Decapitated larvae can undergo initial coiling morphogenesis

The Ihara group reported incredible wound healing activity of *Xenopus* tailbud embryos; even after being cut into two pieces in the mid-trunk region, both the anterior and posterior partial hemi-embryos can survive for several days due to rapid wound healing activity in the amputated area (Yoshii et al., 2005a, b). Inspired by this work, we predicted that the high wound healing activity of *Xenopus* embryos may allow the identification of minimal tissues required for gut coiling morphogenesis. Thus, we first cut off the head region to examine whether the resulting partial embryos can exercise normal coiling morphogenesis. After three series of amputation experiments (Fig. 7A), we concluded that the frontal head region is not essential for gut coiling morphogenesis. In addition, if the heart was intact in the partially decapitated embryos, blood circulation may have promoted gut coiling morphogenesis (Fig. 7C–D, Table 3). Normal coiling was observed in 69 out of 70 decapitated larvae with an intact heart (Fig. 7C), while only 15 out of 71 decapitated larvae without a heart underwent normal coiling morphogenesis (Fig. 7D). Only 4 out of 35 'torso' explants without both head and tail regions underwent coiling morphogenesis (Fig. 7E). However, coiling of the gut was sometimes observed even in torso explants, suggesting that commitment for the initial phase of gut coiling is involved in the nascent gut and occurs during the tailbud stage.

Recapitulating coiling morphogenesis of isolated larval gut explants in vitro

To examine the possibility of gut coiling morphogenesis *in vitro* without complicated interactions with other tissues, we developed a simplified culture method for yolky *Xenopus* early gut tissue (Fig. 8). The gut of stage 41 early larvae is rather straight and not yet coiled, and the gut surface was delaminated from the ventral abdominal muscular layer to demarcate the abdominal cavity. Using

forceps and microscopic scissors, the straight gut was excised at both anterior and posterior ends, and isolated from other parts of the body (Fig. 8A). The isolated gut was cultured for 1 day in 70% diluted CO_2-independent medium. Most of the resulting explants exhibited significant looping (n = 44/48; Fig. 8B–D). This result suggests that by stage 41, gut tissue possessed an intrinsic ability for coiling morphogenesis. In other words, our culture method revealed that the gut can coil to some extent without the aid of the surrounding tissues.

Administration of reagents disrupting actomyosin contraction prevents coiling morphogenesis in the early gut

Using our gut culture system for assessing coiling morphogenesis, we separately administered each of the three reagents that nullify actomyosin contraction of smooth muscle cells (Figs. 9–11). First, we examined the effect of CK-666, an inhibitor of the Arp2/3 complex, which is known to be essential for filamentous actin network formation (Nolen et al., 2009, Hetrik et al., 2013, Ilatovskaya et al., 2013; Fig. 9).

Following administration of CK-666, the ratio of explants displaying looping decreased compared with normal sibling explants not treated with the reagents (Fig. 9G). In explants from normal siblings treated with 0.1% DMSO, 52 out of 71 explants underwent looping, whereas in explants cultured in medium containing 50 μM CK-666, only 29 out of 72 explants showed looping (p <0.01, statistically significant at 1% significance level). Using immunohistochemistry with anti-SM-actin antibody, we confirmed that CK-666 inhibits actin polymerization on the surface of explants (Fig. 9E–F).

Next, ML-9, an inhibitor of MLCK, was administered to isolated gut explants before coiling (Fig. 10). MLCK is known to positively regulate actomyosin contraction via the phosphorylation of myosin light chain to enhance the ATPase activity of myosin (Wang et al., 2007, Várnai et al., 2009, Park et al., 2010). Looping of the early gut was significantly prevented by this reagent (Fig. 10E). In explants from normal siblings treated with 0.1% DMSO, 41 out of 52 underwent looping, whereas in explants cultured in medium containing 50 μM ML-9, only 11 out of 49 showed looping (p <0.01).

Finally, W-7, an antagonist of calmodulin function, was administered to the gut explants before looping (Fig. 11). Calmodulin is known to bind cytoplasmic free Ca^{2+} ions to activate MLCK and thereby facilitate actomyosin contraction in smooth muscle cells (Tanaka and Hidaka 1980, Itoh and Hidaka 1984, Asano 1990). In medium containing 10 μM W-7, only 25 out of 64 gut explants underwent looping after 1 day of culture, whereas in control sibling explants treated with 0.1% DMSO, 46 out of 58 explants showed looping (p <0.01) (Fig. 11E).

Administration of Blebbistatin to the nascent gut explant significantly inhibited the coiling morphogenesis in vitro.

Immersion of the early larvae in the artificial fresh water containing 0.1 μM (±)-Blebbistatin decreased the extent of gut coiling morphogenesis (Fig. 4). However, it is important to answer the criticism that indirect secondary effect targeting the tissues other than the nascent gut perturbed the normal coiling morphogenesis of the gut. Thus, to examine the specific effects of Blebbistatin

treatment only to the nascent gut just before coiling, I performed *in vitro* culture of the gut explant under the inhibition of actomyosin contraction by the administration of the Blebbistatin. In control sibling explants without Blebbistatin, 78% of the samples underwent normal coiling morphogenesis (n=56/72; Fig. 12A). In contrast, gut explants under the inhibition of actomyosin contraction by Blebbistatin, failure of the gut coiling was observed in a dose-dependent manner. By 0.01 μM Blebbistatin treatment, 69% of the specimen caused U-shape or no looping (n=49/71; Fig. 12B). More importantly, 0.05-0.1 μM Blebbistatin treatment strongly abrogated the coiling, and almost all of the specimen caused U-shape or no looping (n=135/144, Fig. 12C–D; $p < 0.01$).

Next, I tried to inhibit Rho kinase activity in the gut explants *in vitro* using the Rho kinase inhibitor Y-27632. Rho kinase activity is known to facilitate filamentous F-actin within the motile cells (Kosako et al., 2000, Wei and Adelstein 2002), and from my above mentioned results, I have had an idea that fine and sequential organization of the gut smooth muscle cells might be under the control of the Rho kinase activity.

Thus I performed the administration of Y-27632 to the gut explants *in vitro*. As a result, Y-27632 completely arrested the gut coiling morphogenesis, and all the explants showed no looping and remained straight shape without the curvature (n= 57/57: $p < 0.01$: Fig.13 C). Here I examined the state of SM-actin in the culture specimen after the administration of Y-27632, by the immunostaining using anti-SM-actin antibody. I found that Y-27632 caused the severe loss of SM-actin organization (n=13/21: Fig.13 B'). Combination of Y-27632 administration and succeeding immunostaining to visualize SM-actin filaments suggests that Rho-kinase activity in essential for the initial gut coiling in *Xenopus* early larvae.

Based on a series of gut explant culture and administration of the reagents targeting actomyosin and related molecules, I propose that spatiotemporally controlled appropriate contraction of actomyosin within the gut smooth muscle cells is indispensable for the orchestrated gut coiling morphogenesis.

Administration of Wnt signaling inhibitor to the nascent gut explant gut in vitro.

Early studies reported that components of the Wnt signaling pathway are expressed in the digestive tract during the organogenic stage in *Xenopus* (Damianitsch et al., 2009). Here, I hypothesized that Wnt signaling might be involved in the gut coiling morphogenesis in *Xenopus* early larvae, thus I examined the effects of Wnt inhibitor on gut explants *in vitro*. Wnt-C59, which is known to inhibit secretion of Wnt ligands by inhibiting the PORCN (Porcupine) activity and arresting palmitoylation of Wnt ligands. By administrating Wnt-C59, all of the three intracellular Wnt signaling cascades are nullified because of the absence of Wnt ligands. In results, administrating 10 μM Wnt-C59 caused significant loss of the looping (Fig. 14B–D, G). 47% of the explants showed U-shaped (n=28/60), and 10% of the explants showed no looping (n=6/60) in the experimental group, whereas most of the control siblings (82%, n=49/60) showed gut coiling after the culture (Fig. 14A, G). The difference of the extent of the looping between the two groups is statistically significant at the 1% significance level ($p < 0.01$). Immunostaining for the isolated gut specimen after the overnight culture with Wnt-

C59 treatment revealed that Wnt-C59 abrogated the formation of SM-actin filaments (n=9/12; Fig. 14F), whereas in control sibling explants, SM-actin filaments formed normally after the 1 day culture (n=8/12; Fig. 14E). These results suggest that Wnt signaling is needed for the SM-actin filament formation in the gut explants, and thus essential for the larval gut coiling morphogenesis.

As mentioned above, Wnt signaling cascade have three intracellular signaling pathways downstream of the trans-membrane receptors. Cardionogen-1 reportedly inhibited the action of Wnt3a and reduced the beta-catenin-dependent transcriptional activities (Ni et al., 2011). I immersed the wholemount late tailbud stage embryos with Cardionogen-1 for 2 days. In consequence, 66% of the individuals showed attenuated gut coiling (n=95/143). It is notable that among the 44 specimens, the larvae after the treatment showed left-right symmetric gut morphology with slight meander only in the dorso-ventral directions (Fig. 15B, D). Immunostaining of the wholemount specimens after the Cardionogen-1 treatment and those of the control siblings revealed that administration of Cardionogen-1 disturbed the meshwork of SM-actin-positive gut smooth muscle cells and its anisotropic twisting was completely lost in the coiling center, which was not observed in control specimens (Fig. 15A"–B").

5. Discussion

In this report, I showed spatiotemporally regulated expression of the smooth muscle-specific actin and sequential orientation behavior of gut smooth muscle cells. Then I employed a pharmacological and explant culture approach to inhibit intestinal myosin II function, and the effects of these reagents on morphogenesis of the gut *in vivo* and *in vitro* were investigated. Myosin isoforms comprise a vast superfamily (Sebé-Pedrós et al., 2014), vertebrate *Xenopus* laevis has at least two non-muscle myosin genes (*myh9* (*myosin IIA*), *myh10*; Kelley et al., 1995; Buisson et al., 2014; Pfister et al., 2016). Myosin IIA is reportedly expressed in *Xenopus* intestine (Session et al., 2016). Based on the obtained results presented in Figs. 2 and 3, I suggested that contraction of actomyosin is essential for gut coiling morphogenesis. Gut tubes form with left-right asymmetry under the control of the *nodal => pitx2* left-right asymmetric genetic cascade (Shinohara and Hamada, 2017; Hamada and Tam, 2020). This left-handed cascade works during the late neurula to mid-tailbud stage (Jones et al., 1995; Sampath et al., 1997; Ryan et al., 1998; Schweickert et al., 2000; Essner et al., 2000; Essner et al., 2002; Essner et al., 2005; Toyoizumi et al., 2005; Schweickert et al., 2007). However, relationships between *pitx2*-dependent establishment of left-right orientation and actual asymmetric morphogenesis of the gut are not fully understood (Noël et al., 2013). The results of my thesis shed light on the role of actomyosin in determining the morphology of the gut in the abdominal cavity.

Implication of the spatiotemporally regulated SM-actin expression and the gut smooth muscle cells' orientation and a series of pharmacological treatments

For normal gut coiling morphogenesis, establishment of regional identities along with both antero-posterior and left-right axes might be needed for region-dependent differentiation of digestive organs (Chalmer and Slack 1998, Matsushita et al., 2002). Expression of Hox genes is essential for antero-posterior regional identity and gut maturation, and Hox expression starts at stage 41 (Lombardo and Slack, 2001). This previous work revealed that *hox a9* and *hox a13* are expressed in the presumptive region of the large intestine. Stage 41 is when the initial gut looping begins as a S-shaped curvature of the yolk-rich gut. The current line of thinking is that the initial S-shape formation does not affect the differential expression of Hox genes, but subsequent gut coiling morphogenesis may be related to Hox expression (Coutelis et al., 2013). As larval development progresses, the ventral pancreas rotates along the gut tube to meet the dorsal pancreas, and both dorsal and ventral pancreatic rudiments fuse to make one pancreas (Suda et al., 1981; Tadokoro et al., 1997). During this process, SM-actin starts to be expressed at stage 41, and smooth muscle cells gradually differentiate to cover the entire surface of the gut tube (Saint-Jeannet et al., 1992).

In the present study, differentiation of smooth muscle cells was examined by whole-mount immunostaining of SM-actin and phosphorylated myosin, and I succeeded in revealing a continuous change in the SM-actin and myosin expression patterns. At first, an SM-actin-positive region arose from the specific site = duodenum, anterior to the ventral pancreas, and this positive region subsequently expands to the entire surface of the gut in a highly reproducible manner, implying genetic control of the distribution of SM-actin (Figs. 1 and 2). I hypothesize that overall control of

hox expression results in an antero-posterior gradient of SM-actin, and this is finely-tuned by the mechanical contraction force generated within the gut tube. I suggest that the characteristic expression pattern of SM-actin presented in this work could generate a gradient of the smooth muscle orientation behavior, based on the coincidental timing of these two events (Fig. 2), and guide coiling morphogenesis of the gut tube. In future studies, I will attempt to inhibit actomyosin contraction precisely and locally via the light-induced release of caged-ATP (Weinreich et al., 1999).

Early investigators reported a wide range of expression patterns for SM-actin in various tissues, and aortic smooth muscle cells and visceral muscles were found to be SM-actin-positive (Saint-Jeannet et al., 1992; Barillot et al., 2008; Shi et al., 2010). However, because previous reports were based on observations of tissue section specimens, the graded expansion of the 'expression wave' of SM-actin presented in the present work was not reported. In my whole-mount pharmacological experiments, Blebbistatin caused impaired alignment of smooth muscle cells and simultaneously obstructed coiling morphogenesis of the gut (Fig. 4C', D', Fig. 6A'). This suggests that expansion of the SM-actin-positive area, coupled with its ubiquitous distribution by the time that coiling morphogenesis is completed, might be essential for the normal coiling pattern. In zebrafish, continuous mechanical tension caused by intestinal smooth muscle contraction was revealed to be the essential factor maintaining the integrity of the intestinal tissue, and disturbance of mechanical tension induced the invasion of epithelial cells through the basal part of the basement membrane (Seiler et al., 2012). I therefore predict that impaired distribution of SM-actin may interfere with the intrinsic tensile stress normally present in the intestinal epithelium, suggesting that Blebbistatin severely diminished the integrity of the epithelium. Womble et al. (2016) proposed that rearrangement of epithelial cells is pivotal for gut looping (Reed et al., 2009). Application of novel tissue clarification technology such as CLARITY might help to illuminate the contribution of the rearrangement of epithelial cells in the *Xenopus* nascent gut (Chung et al., 2013).

On the anisotropic torsion of the stage 45-46 gut smooth muscle meshwork

My CLSM observations revealed that in stage 45–46 larvae (1 week after fertilization), torsion of the gut smooth muscle meshwork occurs in the center of the intestinal coiling region. Considering the contractile nature of the smooth muscle cells, this finding strongly suggests that anisotropic tensile stress is generated in this central region during coiling morphogenesis of the gut. The myosin family consists of numerous members, among which Myosin I interact with actin to generate tensile stress in the plasma membrane to cause tubular coiling morphogenesis in *Drosophila* (Mclntosh and Ostap, 2016). In *Drosophila* embryos, *myosin I* is expressed strongly in the digestive organs (Morgan et al., 1995). Matsuno and colleagues identified the *souther* mutant displaying left-right reversal of the hindgut in *Drosophila*, and the causative gene was found to be *Myo31DF*, encoding *myosin I* (Hozumi et al., 2006). Furthermore, the direction of twisting of the hindgut is determined by the *myosin I*-induced chiral morphology of hindgut epithelial cells. Thus, at least in *Drosophila*, genetically-controlled anisotropic deformation of the gut epithelium is crucial for left-right asymmetric twisting of the hindgut (Hatori et al., 2014).

In vertebrate *Xenopus* embryos, genes encoding myosin family members are expressed in various tissues including somites, brain, eyes, branchial arches, pronephros, heart and gut (Bhatia-Dey et al., 1998; Muller et al., 2003; Latinkić et al., 2004; Reed et al., 2009; England and Loughna, 2013). After morpholino-based knockdown of *myosin I*, the incidence of left-right reversal of the heart and visceral organs is increased (McDowell et al., 2016). The consistency between *Drosophila* and *Xenopus* embryos implies that some evolutionarily conserved myosin I-related mechanism might control left-right asymmetric coiling morphogenesis in both protostomes and deuterostomes. However, roles of myosin II in embryonic/larval organogenesis have not yet fully analyzed in *Xenopus*, possibly because of the multiple expression pattern from very early embryonic stages make it difficult to interpret the results of knock-down/knock-out experiments, or else such loss-of-function experiments have a risk to induce severe phenotype leading to embryonic lethality. In such a situation, experimental strategy using pharmacological reagents might be effective to decode the role of myosin II in later stage organogenesis.

Because clear torsion of SM-actin-positive smooth muscle cells was observed in stage 46 early larvae, some tensile stress within the gut tissue might drive coiling morphogenesis of it. Like the spiral shells of snails, coiling morphogenesis of the anuran gut results in a defined spiral loop. The smooth muscle meshwork forms precise longitudinal and transverse filaments along the gut outside the central area (Fig. 2). Thus, I propose that appropriate contractile twisting force at precise timing of differentiating gut smooth muscle cells might participate in coiling morphogenesis in addition to the effects by epithelial cell rearrangements (Muller et al., 2003, Reed et al., 2009). Voluntary and subsequent peristaltic contraction of gut muscular cells may act as coordinators to orchestrate the spiral coiling pattern. In summary, I propose that appropriate contraction of developing gut smooth muscle cells is needed to generate the normal coiling pattern during *Xenopus* gut coiling morphogenesis.

Decapitation at the tail bud stage does not affect the gut coiling pattern

To examine the possibility that the central nervous system controls the gut coiling morphogenesis pattern, I performed a series of amputation experiments. The results showed that when the heart was preserved in the decapitated embryo, the normal gut coiling pattern was retained in larvae up to stage 46 (Fig. 7C, Table 3). Amputation of both the head and heart decreased the probability of successful coiling, suggesting that blood circulation is helpful in further promoting the coiling process (Fig. 7C–D). Additionally, short explants resulting from amputation of both head and tail regions could curve to some extent, and in most successful larvae, the stage 44 initial gut coiling pattern was recapitulated in these torso explants (Fig. 7E). Therefore, even though fine-tuning of the coiling pattern may be a prerequisite for correct looping and coiling, the *Xenopus* larval gut can undergo initial left-right asymmetric coiling without the aid of other parts of the body, including the central nervous system.

Development of isolated gut explants indicates tissue-autonomous coiling morphogenesis of the gut

Using my newly developed technique, *Xenopus* larval isolated gut samples could recapitulate

coiling morphogenesis *in vitro* (Fig. 8). Thus, I concluded that information for coiling is encoded in the gut tissue until stage 41 of dissection and isolation. Gut coiling is, therefore, a gut-autonomous phenomenon thereafter. Treatment with either CK-666 (actin polymerization inhibitor), ML-9 (MLCK inhibitor), or W-7 (calmodulin antagonist) decreased the extent of looping, suggesting that actomyosin contraction is essential for coiling morphogenesis (Figs. 9, 10, and 11). However, I could not recapitulate late stage gut coiling that normally occurs during stages 44–46 using my culture conditions, suggesting that mechanisms for gut coiling during the later stages are somewhat different from those operating during the initial looping at stage 41–43. I could not induce longitudinal filament formation in my explants. After 1 day of culture, gut explants formed SM-actin filaments only in the transverse direction *in vitro* (Fig. 8E), while in earlier stage 43 larvae, whole-mount specimens exhibited filament formation only in the transverse direction (Figs. 2C, K and 3 A–C). This similarity suggests that gut coiling during stages 44–46 requires longitudinal SM-actin filament formation coupled with transverse filaments (Fig. 2E-K).

Heart tube explant experiments on zebrafish embryos revealed that looping of the heart requires actomyosin contraction, and the directionality of the looping is guided by left-handed *nodal* expression (Noël et al., 2013). Although early studies are confined only to teleosts (zebrafish), the results suggest that left-handed *nodal* expression has some genetic linkage with actomyosin contraction. Herein, pharmacological treatment of amphibian *Xenopus* larvae often caused abrogation of gut left-right asymmetry, which is generally interpreted as a loss of left-right asymmetric information. Thus, I propose that in vertebrates, at the end of the left-right asymmetric genetic cascade downstream of the left-handed *pitx2*, actomyosin might act as an effector in determining gut morphology (Ryan et al., 1998; Schweickert et al., 2000; Essner et al., 2000; Horne-Badovinac et al., 2003; Hochgreb-Hägele et al., 2013).

Wnt signaling pathway may be involved in controlling gut coiling morphogenesis.

I explored the mechanisms generating the highly-organized smooth muscle cellular meshwork. I speculate that some unknown secretory factor(s) may induce formation of the meshwork. I focused on Wnt signaling because the Wnt signaling cascade includes myosin-related players in its downstream part. Wnt signaling comprises three intracellular signaling pathways: the canonical pathway, the planar cell polarity (PCP) pathway, and the Ca^{2+}-dependent pathway. In the non-canonical Wnt pathways, Rho kinase activates the accumulation of myosin II molecules (Sokol., 2015). In cultured mammalian kidney glomerular epithelium cells, activation of Wnt signaling potentiates the formation of F-actin stress fibers and changes the cell morphology (Babayeba et al., 2010). Early investigators reported that accumulation of myosin II activates the formation of stress fibers, resulting in the deformation of epithelial cells (Lapébie et al., 2011). In the present study, administration of Wnt C-59, a Wnt signaling pathway inhibitor, inhibits gut coiling and polymerization of SM-actin *in vitro* (Fig. 14 C-D, F). This suggests that Wnt signaling is needed for the gut coiling morphogenesis at the early larval stage. Moreover, by administration of Cardionogen-1, a Wnt signaling canonical pathway modulator, inhibit gut coiling morphogenesis and smooth

muscle cellular meshwork (Fig. 15 B, D, F). Accumulating evidence indicates that Wnt signaling may be directly involved in mediating looping morphogenesis in the developing gut.

Concluding remarks: Intestinal actomyosins can reveal evolutionary aspects of the left-right asymmetry of vertebrate visceral organs

In *Xenopus*, coiling morphogenesis of the larval gut can be nullified if the contraction force in juvenile gut cells is inhibited. Thus, the contraction force during early larval stages is essential for normal coiling morphogenesis. In future work, I hope to expand our knowledge concerning the role of actomyosin in vertebrate organ morphogenesis. Metazoan animals often employ a 'co-option' strategy during development (Irie and Kuratani, 2011; Hall and Gillis, 2013). In many organ systems, versatile signaling pathways are repeatedly used for organogenesis, hence I predict that the actomyosin system may also be co-opted in many morphogenic systems in various animals. Because the myosin family includes many members, knowing which family members participate in visceral organ morphogenesis in each class of vertebrates could help us to understand the evolutionary conservation and diversification of the role of myosin in organ morphogenesis. In the future, actomyosin could prove to be a fascinating macromolecular complex not only for cell biology, but also for evolutionary developmental biology.

6. Acknowledgements

I thank Prof. Yoshitaka Azumi for fruitful discussions and detailed technical advice. I also thank Prof. Susumu Kotani, Prof. Susumu Izumi, Prof. Ken'ichi Kanazawa, and Prof. Tsuyoshi Ohira from Kanagawa University for numerous discussions, fruitful advice, and encouragement. I am deeply thankful to Dr. Kazue Mogi (Kanagawa University) and Shinya Tsuruoka (Kanagawa University) for technical advice on molecular embryology techniques. I also thank Prof. Hideho Uchiyama (Yokohama City University) for providing a protocol for *Xenopus* immunostaining. This work was supported by a Grant-in-Aid of Kanagawa University Collaborative Research (2019-No. 2).

7. Reference

Asano M., 1990. Effects of the calmodulin antagonist W-7 on isometric tension development and myosin light chain phosphorylation in bovine tracheal smooth muscle. Jpn J Pharmacol. 52:471-81.

Babayeva S, Rocque B, Aoudjit L, Zilber Y, Li J, Baldwin C, Kawachi H, Takano T, & Torban E. (2013). Planar cell polarity pathway regulates nephrin endocytosis in developing podocytes. J Biol Chem, 288(33), 24035-24048. doi: 10.1074/jbc.M113.452904. Epub 2013 Jul 3. PMID: 23824190

Barillot W, Tréguer K, Faucheux C, Fédou S, Thézé N, Thiébaud P. Induction and modulation of smooth muscle differentiation in Xenopus embryonic cells. Dev Dyn. 2008 Nov;237(11):3373-86. doi: 10.1002/dvdy.21749. PMID: 18855898

Blum M, Ott T., 2018. Animal left-right asymmetry. Curr Biol. 28: R301-R304.

Buisson N, Sirour C, Moreau N, Denker E, Le Bouffant R, Goullancourt A, Darribère T, Bello V. An adhesome comprising laminin, dystroglycan and myosin IIA is required during notochord development in Xenopus laevis. Development. 2014 Dec;141(23):4569-79. doi: 10.1242/dev.116103. Epub 2014 Oct 30. PMID: 25359726

Campione M, Steinbeisser H, Schweickert A, Deissler K, van Bebber F, Lowe LA, Nowotschin S, Viebahn C, Haffter P, Kuehn MR, Blum M., 1999. The homeobox gene Pitx2: mediator of asymmetric left-right signaling in vertebrate heart and gut looping. Development. 126:1225-34.

Chalmers AD, Slack JM. Development of the gut in Xenopus laevis. Dev Dyn. 1998 Aug;212(4):509-21. doi: 10.1002/(SICI)1097-0177(199808)212:4<509::AID-AJA4>3.0.CO;2-L. PMID: 9707324

Chung K, Wallace J, Kim SY, Kalyanasundaram S, Andalman AS, Davidson TJ, Mirzabekov JJ, Zalocusky KA, Mattis J, Denisin AK, Pak S, Bernstein H, Ramakrishnan C, Grosenick L, Gradinaru V, Deisseroth K., 2013. Structural and molecular interrogation of intact biological systems. Nature. 2013 497:332-7.

Coutelis JB, Géminard C, Spéder P, Suzanne M, Petzoldt AG, Noselli S., 2013. Drosophila left/right asymmetry establishment is controlled by the Hox gene abdominal-B. Dev Cell. 24:89-97.

Damianitsch K, Melchert J, Pieler T. XsFRP5 modulates endodermal organogenesis in Xenopus laevis. Dev Biol. 2009 May 15;329(2):327-37. doi: 10.1016/j.ydbio.2009.03.004. Epub 2009 Mar 12. PMID: 19285490

Davis NM, Kurpios NA, Sun X, Gros J, Martin JF, Tabin CJ., 2008. The chirality of gut rotation derives from left right asymmetric changes in the architecture of the dorsal mesentery. Dev Cell. 15: 134-45.

Dasgupta M., 2004. Relative length of the gut of some freshwater fishes of West Bengal in relation to food and feeding habits Corpus ID: 86898595. Semantic scholar Published 2004

England J, Loughna S., 2013. Heavy and light roles: myosin in the morphogenesis of the heart. Cell Mol Life Sci. 70:1221-39.

Essner JJ, Amack JD, Nyholm MK, Harris EB, Yost HJ., 2005. Kupffer's vesicle is a ciliated organ of asymmetry in the zebrafish embryo that initiates left-right development of the brain, heart and gut. Development. 132:1247-60.

Essner JJ, Branford WW, Zhang J, Yost HJ., 2000. Mesendoderm and left-right brain, heart and gut development are differentially regulated by pitx2 isoforms. Development. 127:1081-93.

Essner JJ, Vogan KJ, Wagner MK, Tabin CJ, Yost HJ, Brueckner M., 2002. Conserved function for embryonic nodal cilia. Nature. 418:37-8.

Georgijevic S, Subramanian Y, Rollins EL, Starovic-Subota O, Tang AC, Childs SJ. Spatiotemporal expression of smooth muscle markers in developing zebrafish gut. Dev Dyn. 2007 Jun;236(6):1623-32. doi: 10.1002/dvdy.21165. PMID: 17474123

Hall BK, Gillis JA., 2013. Incremental evolution of the neural crest, neural crest cells and neural crest-derived skeletal tissues. J Anat. 222:19-31.

Hamada H, Tam P., 2020. Diversity of left-right symmetry breaking strategy in animals. F1000Res. 19;9:F1000 Faculty Rev-123.

HAMBURGER V, HAMILTON HL., 1951. A series of normal stages in the developent of the chick embryo. J Morphol. 88:49-92.

Hatori R, Ando T, Sasamura T, Nakazawa N, Nakamura M, Taniguchi K, Hozumi S, Kikuta J, Ishii M, Matsuno K., 2014. Left-right asymmetry is formed in individual cells by intrinsic cell chirality. Mech Dev. 133: 146-62.

Hetrick B, Han MS, Helgeson LA, Nolen BJ., 2013. Small molecules CK-666 and CK-869 inhibit actin-related protein 2/3 complex by blocking an activating conformational change. Chem Biol. 20:701-12.

Hochgreb-Hägele T, Yin C, Koo DE, Bronner ME, Stainier DY., 2013. Laminin β1a controls distinct steps during the establishment of digestive organ laterality. Development. 140:2734- 45.

Horne-Badovinac S, Rebagliati M, Stainier DY., 2003. A cellular framework for gut- looping morphogenesis in zebrafish. Science. 302:662-5.

Hozumi S, Maeda R, Taniguchi K, Kanai M, Shirakabe S, Sasamura T, Spéder P, Noselli S, Aigaki T, Murakami R, Matsuno K., 2006. An unconventional myosin in Drosophila reverses the default handedness in visceral organs. Nature. 440:798-802.

Ilatovskaya DV, Chubinskiy-Nadezhdin V, Pavlov TS, Shuyskiy LS, Tomilin V, Palygin O,

Staruschenko A, Negulyaev YA., 2013. Arp2/3 complex inhibitors adversely affect actin cytoskeleton remodeling in the cultured murine kidney collecting duct M-1 cells. Cell Tissue Res. 354:783-92.

Irie N, Kuratani S., 2011. Comparative transcriptome analysis reveals vertebrate phylotypic period during organogenesis. Nat Commun. 2:248.

Itoh H, Hidaka H., 1984. Direct interaction of calmodulin antagonists with Ca2+/calm- odulin-dependent cyclic nucleotide phosphodiesterase. J Biochem. 96:1721-6.

Iwaki DD, Johansen KA, Singer JB, Lengyel JA., 2001. drumstick, bowl, and lines are required forpatterning and cell rearrangement in the Drosophila embryonic hindgut. Dev Biol. 240:611-26.

Jones CM, Kuehn MR, Hogan BL, Smith JC, Wright CV., 1995. Nodal-related signals induce axial mesoderm and dorsalize mesoderm during gastrulation. Development. 121:3651-62. PMID: 8582278

Kampourakis T, Zhang X, Sun YB, Irving M., 2018. Omecamtiv mercabil and blebbistatin modulate cardiac contractility by perturbing the regulatory state of the myosin filament. J Physiol. 596:31-46.

Kato Y, Miyakawa T, Tanokura M., 2018. Overview of the mechanism of cytoskeletal motors based on structure. Biophys Rev. 10:571-581.

Kelley CA, Adelstein RS. Characterization of myosin II isoforms containing insertions of amino acids in the flexible loop near the ATP-binding pocket. Biophys J. 1995 Apr;68(4 Suppl):225S. PMID: 7787079

Kovács M, Tóth J, Hetényi C, Málnási-Csizmadia A, Sellers JR., 2004. Mechanism of blebbistatin inhibition of myosin II. J Biol Chem. 279:35557-63.

Kosako H, Yoshida T, Matsumura F, Ishizaki T, Narumiya S, Inagaki M. Rho-kinase/ROCK is involved in cytokinesis through the phosphorylation of myosin light chain and not ezrin/radixin/moesin proteins at the cleavage furrow. Oncogene. 2000 Dec 7;19(52):6059-64. doi: 10.1038/sj.onc.1203987. PMID: 11146558

Lapébie P, Borchiellini C, & Houliston E. (2011). Dissecting the PCP pathway: one or more pathways?: Does a separate Wnt-Fz-Rho pathway drive morphogenesis? Bioessays, 33(10), 759-768. doi: 10.1002/bies.201100023. Epub 2011 Aug 23. PMID: 21919026

Latinkic BV, Cooper B, Smith S, Kotecha S, Towers N, Sparrow D, Mohun TJ., 2004. Transcriptional regulation of the cardiac-specific MLC2 gene during Xenopus embryonic development. Development.

131:669-79.

Lombardo A, Slack JM., 2001. Abdominal B-type Hox gene expression in *Xenopus laevis*. Mech Dev. 106:191-5.

Manstein DJ., 2004. Molecular engineering of myosin. Philos Trans R Soc Lond B Biol Sci. 359:1907-12.

Marston DJ, Goldstein B., 2006. Actin-based forces driving embryonic morphogenesis in Caenorhabditis elegans. Curr Opin Genet Dev. 16:392-8.

Matsushita S, Ishii Y, Scotting PJ, Kuroiwa A, Yasugi S. Pre-gut endoderm of chick embryos is regionalized by 1.5 days of development. Dev Dyn. 2002 Jan;223(1):33-47. doi: 10.1002/dvdy.1229. PMID: 11803568

Ma X, Adelstein RS., 2012. In vivo studies on nonmuscle myosin II expression and function in heart development. Front Biosci (Landmark Ed). 17:545-55.

McDowell GS, Lemire JM, Paré JF, Cammarata G, Lowery LA, Levin M., 2016. Conserved roles for cytoskeletal components in determining laterality. Integr Biol (Camb). 8:267-86.

McIntosh BB, Ostap EM., 2016. Myosin-I molecular motors at a glance. J Cell Sci. 129: 2689-95.

Morgan NS, Heintzelman MB, Mooseker MS., 1995. Characterization of myosin-IA and myosin-IB, two unconventional myosins associated with the Drosophila brush border cytoskeleton. Dev Biol. 172:51-71.

Muller JK, Prather DR, Nascone-Yoder NM. Left-right asymmetric morphogenesis in the Xenopus digestive system. Dev Dyn. 2003 Dec;228(4):672-82. doi: 10.1002/dvdy.10415. PMID: 14648844

Nerurkar NL, Mahadevan L, Tabin CJ., 2017. BMP signaling controls buckling forces to modulate looping morphogenesis of the gut. Proc Natl Acad Sci U S A. 114:2277-2282.

Ni TT, Rellinger EJ, Mukherjee A, Xie S, Stephens L, Thorne CA, Kim K, Hu J, Lee E, Marnett L, Hatzopoulos AK, Zhong TP. Discovering small molecules that promote cardiomyocyte generation by modulating Wnt signaling. Chem Biol. 2011 Dec 23;18(12):1658-68. doi: 10.1016/j.chembiol. 2011.09.015. PMID: 22195568

Nie W, Wei MT, Ou-Yang HD, Jedlicka SS, Vavylonis D., 2015. Formation of contractile networks

and fibers in the medial cell cortex through myosin-II turnover, contraction, and stress-stabilization. Cytoskeleton (Hoboken). 72:29-46.

Nieuwkoop PD, Faber J, 1967. Normal table of Xenopus laevis (Daudin). Routledge, Abingdon

Noël ES, Verhoeven M, Lagendijk AK, Tessadori F, Smith K, Choorapoikayil S, den Hertog J, Bakkers J., 2013. A Nodal-independent and tissue-intrinsic mechanism controls heart-looping chirality. Nat Commun. 4: 2754.

Nolen BJ, Tomasevic N, Russell A, Pierce DW, Jia Z, McCormick CD, Hartman J, Sakowicz R, Pollard TD., 2009. Characterization of two classes of small molecule inhibitors of Arp2/3 complex. Nature. 460:1031-4.

Okumura T, Sasamura T, Inatomi M, Hozumi S, Nakamura M, Hatori R, Taniguchi K, Nakazawa N, Suzuki E, Maeda R, Yamakawa T, Matsuno K., 2015. Class I myosins have overlapping and specialized functions in left-right asymmetric development in Drosophila. Genetics. 199:1183-99.

Park SY, Shim JH, Kim M, Sun YH, Kwak HS, Yan X, Choi BC, Im C, Sim SS, Jeong JH, Kim IK, Min YS, Sohn UD., 2010. MLCK and PKC Involvements via Gi and Rho A Protein in Contraction by the Electrical Field Stimulation in Feline Esophageal Smooth Muscle. Korean J Physiol Pharmacol. 14(1):29-35.

Perrin BJ, Ervasti JM., 2010. The actin gene family: function follows isoform. Cytoskeleton (Hoboken). 67:630-4.

Pfister K, Shook DR, Chang C, Keller R, Skoglund P. Molecular model for force production and transmission during vertebrate gastrulation. Development. 2016 Feb 15;143(4):715-27. doi: 10.1242/dev.128090. PMID: 26884399

Reed RA, Womble MA, Dush MK, Tull RR, Bloom SK, Morckel AR, Devlin EW, Nascone-Yoder NM., 2009. Morphogenesis of the primitive gut tube is generated by Rho/ROCK/myosin II-mediated endoderm rearrangements. Dev Dyn. 238:3111-25.

Ryan AK, Blumberg B, Rodriguez-Esteban C, Yonei-Tamura S, Tamura K, Tsukui T, de la Peña J, Sabbagh W, Greenwald J, Choe S, Norris DP, Robertson EJ, Evans RM, Rosenfeld MG, Izpisúa Belmonte JC., 1998. Pitx2 determines left-right asymmetry of internal organs in vertebrates. Nature. 394:545-51.

Saint-Jeannet JP, Levi G, Girault JM, Koteliansky V, Thiery JP., 1992. Ventrolateral regionalization

of Xenopus laevis mesoderm is characterized by the expression of alpha-smooth muscle actin. Development. 115: 1165-73.

Schneider A, Mijalski T, Schlange T, Dai W, Overbeek P, Arnold HH, Brand T., 1999. The homeobox gene NKX3.2 is a target of left-right signalling and is expressed on opposite sides in chick and mouse embryos. Curr Biol. 9:911-4.

Schweickert A, Campione1 M, Steinbeisser H, Blum M. Pitx2 isoforms: involvement of Pitx2c but not Pitx2a or Pitx2b in vertebrate left-right asymmetry. Mech Dev. 2000 Jan;90(1):41-51. doi: 10.1016/s0925-4773(99)00227-0. PMID: 10585561

Schweickert A, Weber T, Beyer T, Vick P, Bogusch S, Feistel K, Blum M., 2007. Cilia-driven leftward flow determines laterality in Xenopus. Curr Biol. 17: 60-6.

Sebé-Pedrós A, Grau-Bové X, Richards TA, Ruiz-Trillo I. (2014). Evolution and classification of myosins, a paneukaryotic whole-genome approach. Genome Biol Evol. 6:290-305.

Seiler C, Davuluri G, Abrams J, Byfield FJ, Janmey PA, Pack M., 2012. Smooth muscle tension induces invasive remodeling of the zebrafish intestine. PLoS Biol. 10: e1001386.

Session AM, Uno Y, Kwon T, Chapman JA, Toyoda A, Takahashi S, Fukui A, Hikosaka A, Suzuki A, Kondo M, van Heeringen SJ, Quigley I, Heinz S, Ogino H, Ochi H, Hellsten U, Lyons JB, Simakov O, Putnam N, Stites J, Kuroki Y, Tanaka T, Michiue T, Watanabe M, Bogdanovic O, Lister R, Georgiou G, Paranjpe SS, van Kruijsbergen I, Shu S, Carlson J, Kinoshita T, Ohta Y, Mawaribuchi S, Jenkins J, Grimwood J, Schmutz J, Mitros T, Mozaffari SV, Suzuki Y, Haramoto Y, Yamamoto TS, Takagi C, Heald R, Miller K, Haudenschild C, Kitzman J, Nakayama T, Izutsu Y, Robert J, Fortriede J, Burns K, Lotay V, Karimi K, Yasuoka Y, Dichmann DS, Flajnik MF, Houston DW, Shendure J, DuPasquier L, Vize PD, Zorn AM, Ito M, Marcotte EM, Wallingford JB, Ito Y, Asashima M, Ueno N, Matsuda Y, Veenstra GJ, Fujiyama A, Harland RM, Taira M, Rokhsar DS., 2016. Genome evolution in the allotetraploid frog Xenopus laevis. Nature. 538:336-343.

Shi ZD, Abraham G, Tarbell JM., 2010. Shear stress modulation of smooth muscle cell marker genes in 2-D and 3-D depends on mechanotransduction by heparan sulfate proteoglycans and ERK1/2. PLoS One. 5: e12196.

Shinohara K, Hamada H., 2017. Cilia in Left-Right Symmetry Breaking. Cold Spring Harb Perspect Biol. 9(10): a028282.

Sokol SY. Spatial and temporal aspects of Wnt signaling and planar cell polarity during vertebrate

embryonic development. Semin Cell Dev Biol. 2015 Jun;42:78-85. doi: 10.1016/j.semcdb. 2015.05.002. Epub 2015 May 15. PMID: 25986055

Somu Koundal, Rani Dhanze, Arun Koundal, Indu Sharma., 2012. RELATIVE GUT LENGTH AND GASTRO-SOMATIC INDEX OF SIX HILL STREAM FISHES, HIMACHAL PRADESH, INDIA ResearchGate. August 2012.

Suda K, Mizuguchi K, Hoshino A., 1981. Differences of the ventral and dorsal anlagen of pancreas after fusion. Acta Pathol Jpn. 31:583-9.

Tadokoro H, Kozu T, Toki F, Kobayashi M, Hayashi N., 1997. Embryological fusion between the ducts of the ventral and dorsal primordia of the pancreas occurs in two manners. Pancreas. 14: 407-14.

Tanaka T, Hidaka H., 1980. Hydrophobic regions function in calmodulin -enzyme(s) interactions. J Biol Chem. 255:11078-80.

Taniguchi K, Hozumi S, Maeda R, Okumura T, Matsuno K., 2007. Roles of type I myosins in Drosophila handedness. Fly (Austin). 1:287-90.

Tingler M, Kurz S, Maerker M, Ott T, Fuhl F, Schweickert A, LeBlanc-Straceski JM, Noselli S, Blum M., 2018. A Conserved Role of the Unconventional Myosin 1d in Laterality Determination. Curr Biol. 28:810-816.e3.

Toyoizumi R, Ogasawara T, Takeuchi S, Mogi K., 2005. Xenopus nodal related-1 is indispensable only for left-right axis determination. Int J Dev Biol. 49:923-38.

Várnai P, Hunyady L, Balla T., 2009. STIM and Orai: the long-awaited constituents of store-operated calcium entry. Trends Pharmacol Sci. 30:118-28.

Wang J, Weigand L, Foxson J, Shimoda LA, Sylvester JT., 2007. Ca2+ signaling in hypoxic pulmonary vasoconstriction: effects of myosin light chain and Rho kinase antagonists. Am J Physiol Lung Cell Mol Physiol. 293:L674-85.

Wei Q, Adelstein RS. Pitx2a expression alters actin-myosin cytoskeleton and migration of HeLa cells through Rho GTPase signaling. Mol Biol Cell. 2002 Feb;13(2):683-97. doi: 10.1091/mbc.01-07-0358. PMID: 11854422

Weinreich F, Riordan JR, Nagel G., 1999. Dual effects of ADP and adenylylimidodiphosphate on

CFTR channel kinetics show binding to two different nucleotide binding sites. J Gen Physiol. 114 :55-70.

Womble M, Pickett M, Nascone-Yoder N., 2016. Frogs as integrative models for understanding digestive organ development and evolution. Semin Cell Dev Biol. 51:92-105.

Yoshii Y, Noda M, Matsuzaki T, Ihara S., 2005. Wound healing ability of Xenopus laevis embryos. I. Rapid wound closure achieved by bisectional half embryos.Dev Growth Differ. 47:553-61.

Yoshii Y, Matsuzaki T, Ishida H, Ihara S. Wound healing ability of Xenopus laevis embryos. II. Morphological analysis of wound marginal epidermis. Dev Growth Differ. 2005 Oct;47(8):563-72. doi: 10.1111/j.1440-169X.2005.00831.x.PMID: 16287487

8. Figure Legends and Table Captions

Figure 1

Normal coiling morphogenesis of the *Xenopus* larval gut and stage-dependent expansion of the SM-actin-positive region.

(A and A') The *Xenopus* early larval yolky gut tube begins to curve and forms a S-shape when viewed from the ventral side at stage 42 (A), during which the most anterior gut domain expresses SM-actin (arrowhead in A'). (B and B') At stage 43, the SM-actin-positive domain (duodenum; arrowhead in B') shifts significantly toward the anterior-right portion in accordance with movement driven by gut looping. (C and C') At stage 44, in addition to the first expression in the narrow duodenum (arrowhead in C'), the central turn of the coiling (arrow in C') also expresses SM-actin. (D–D' and E–E') Central expression of SM-actin, which is more intense at the turning point, is subsequently maintained during stage 45–46. All panels are viewed from the ventral side. Scale bars = 200 μm.

Figure 2

Stage-dependent organization of SM-actin-positive cells leading to cellular meshwork formation in the gut region of early *Xenopus* larvae.

Confocal laser-scanning microscopy (CLSM) was performed to observe the 3D distribution of SM-actin, as revealed by immunohistochemistry using anti-SM-actin antibody. (A, B) In stage 41–42 larvae, SM-actin-positive cells are not organized in the central gut, and the expression level is faint. (C, D) In stage 43 larvae, transverse cellular orientation of the smooth muscle cells is first recognized in the thin duodenum (C), while the stout posterior gut has no cellular orientation (D). (E, F) In stage 44 larvae, longitudinal cellular orientation is first observed along the gut tube in the anterior gut in both the duodenum and the coiling center (E). In the posterior gut, only transverse cellular alignment is formed across the gut (F), indicating that an anterior-to-posterior gradient influences the timing of the smooth muscle organization, and transverse cellular orientation is first established before the subsequent longitudinal cellular orientation. (G) In stage 45 larvae, local twisting of SM-actin-positive cellular meshwork is first recognized in the central intestine. (H, I, J) Also, in the stage 46 gut, local anisotropic twisting of SM-actin meshwork occurs at the center of the intestinal coil. In most parts of the gut tube, except for the coiling center, longitudinal and transverse cells are orthogonal to each other. By contrast, anisotropic twisting of the cellular meshwork occurs only in the central coiling region. Panels H and I are photographs of the same larva, while panel J is from another larva. This local twisting is observed in both larvae (H–I and J). (K) Trace of the longitudinal SM-actin-positive cells (green lines) and transverse cells (blue lines) in the central twisted site in J. Line drawings of st. 43–44 larvae also depict orientations of transverse cells (green lines) and longitudinal cells (blue lines). These photographs were taken with an inverted confocal laser-scanning microscope, and the left-right orientations are inverted in these figures to match the left-right orientation in Fig. 1. Scale bars = 100 μm.

Figure 3

Stage-dependent organization of phosphorylated-myosin-positive cells resulting in cellular meshwork formation in the gut region of early *Xenopus* larvae.

CLSM observation was performed to reconstruct 3D distribution of phosphorylated myosin light chain (p-MLC), as was revealed by immunohistochemistry using anti-phospho-myosin light chain antibody. (A, B) In stage 43 larvae, transverse p-MLC-positive cellular alignment is first evident in the duodenum. (D, E) In stage 44 larvae, p-MLC-positive cells start to align along the longitudinal axis of the gut tube in both the duodenum and the coiling center. (G, H) In stage 45–46 larvae, p-MLC-positive cellular meshwork is organized in the coiling center of the gut. (C, F, I) Schematic illustrations for the patterns of p-MLC-positive cellular orientations in the gut tube (Red line) in accordance with the progress of the developmental stage. Blue squares demarcate the scope of CLSM observations. Scale Bars; 100 μm in A, D and G; 40 μm in B, E and H.

Figure 4

Administration of (±)-Blebbistatin (a commonly used myosin II inhibitor) inhibits gut coiling morphogenesis.

(A–A') Immediately after (±)-Blebbistatin treatment, the outer region of treated larvae (A') is essentially identical to that of untreated larvae (A). (B–B', C–C'') After removing (±)-Blebbistatin by washing followed by 2 days of incubation until control siblings reached stage 46, gut coiling morphogenesis was perturbed, and in numerous cases, only the dorso-ventral meander of the gut was observed (B', C'). In other cases, the extent of coiling was less advanced. (D-D') Administration of Blebbistatin from stage 43–44 during coiling morphogenesis arrested further coiling process for 1 day or more, as compared to the control siblings that underwent normal coiling process. Scale bars are 1 mm for A–A', 0.5 mm for B–B', and 200 μm for C–C', D-D'.

Figure 5

Clear differences between Blebbistatin optical isomers demonstrates the essential pharmacological effect of S-(–)-Blebbistatin in *Xenopus* larvae.

Late stage embryos (stage 38–39) were immersed in either R-(+)-Blebbistatin or S-(–)-Blebbistatin for 6 h at a concentration of 0.05 or 0.1 μM. (A and B) After rearing for 2 days, R-(+)-Blebbistatin-treated stage 46 larvae are normal in terms of outer morphology and internal organs. (C) By contrast, S-(–)-Blebbistatin-treated larvae exhibit abrogation or attenuation of gut coiling, demonstrating that, like in mammals (Straight et al., 2003), only the S-(–)-Blebbistatin isomer is effective in *Xenopus*, and only S-(–)-Blebbistatin is essential in racemic (±)-Blebbistatin (Table 2). This result suggests that the target of (±)-Blebbistatin and S-(–)-Blebbistatin is myosin II (Straight et al., 2003; Reed et al., 2009). Scale bars, 200 μm.

Figure 6

Exposure to Blebbistatin perturbs the alignment of SM-actin-positive smooth muscle cells.

(A–A') In normal untreated larvae, the orthogonal meshwork consisting of the longitudinal and

transverse alignment of SM-actin positive cells is established by stage 46 (A). By contrast, intestines of Blebbistatin-treated larvae have disordered meshwork (A'). Counterstaining was performed with CellMask® to visualize the plasma membrane. (B–B') Immunostaining using 12/101 antibody for skeletal muscle revealed that Blebbistatin treatment did not perturb normal myotome formation in the tail region. Panels in Fig. 6 suggest that actomyosin contraction activity during the coiling period is needed for the normal alignment of early intestinal smooth muscle cells. Scale bars are 50 μm for A–A' and 1 mm for B–B'.

Figure 7

Amputated partial larvae can undergo normal gut coiling, especially when the heart and blood circulation are intact.

(A) Design of the three series of amputation experiments. (i) Decapitation of the frontal head was performed at stage 32–33 (tailbud stage). (ii) Decapitation of the head and removal of the heart were also performed at the same stage. (iii) Torso-like partial embryos without the head, heart, and tail regions were prepared and reared. (B) A stage 46 normal sibling larva in a control experiment for comparison. (C) A decapitated larva with an intact heart that underwent normal gut coiling. (D) A decapitated larva without a heart showing incomplete coiling morphogenesis of the gut. (E) Attenuated coiling morphogenesis of a 'torso' partial larva. The pattern of coiling is abnormal, but even in 'torso' larvae, gut curvature was sometimes significant and partially reminiscent of the normal coiling pattern, which inspired us to perform the gut explant culture experiments in Figs. 8–14.

Figure 8

Isolated straight gut explants coiled autonomously after 1 day of culture.

(A) Dissection and isolation of gut tissue after removing both the thoracic and anal regions using microscissors. The photograph in A shows the immature gut immediately after removal.

(B–D) Early larval straight gut explants were isolated and cultured in 70% diluted CO_2-independent medium. Two successful gut coiling morphogenesis cases are shown in B–C, corresponding to the blue stripe in D showing the proportion of successful coiling cases. Scale bars = 500 μm.

Figure 9

CK-666, an inhibitor of actin filament formation, perturbs looping of isolated gut explants.

(A–D) The extent of the looping was greatly reduced following CK-666 treatment, and in many samples the isolated gut only formed a U-shape (C), as shown in the lower orange stripe in G, compared with control explants from siblings (A). (E–F) Immunostaining of SM-actin showing that CK-666 inhibited the polymerization of SM-actin filaments (F). Scale bars are 500 μm for A–D, and 100 μm for E–F.

Figure 10

ML-9, an inhibitor of myosin light chain kinase (MLCK), perturbs coiling morphogenesis of isolated

gut explants.
(B–E) ML-9 greatly reduced the probability of successful looping of the isolated gut after 1 day of culture (E). This suggests that actomyosin interaction-mediated contraction is essential for gut looping. MLCK might be a positive regulator of actomyosin interaction in smooth muscle cells. Control experiments were performed using siblings (A). Scale bars = 500 μm.

Figure 11
W-7, a calmodulin antagonist, prevents coiling morphogenesis in isolated gut explants.
(B–E) W-7 decreased the probability of successful looping of the isolated gut after 1 day of culture (E). Control experiments were performed using siblings (A). Scale bars = 500 μm.

Figure 12
Blebbistatin, an inhibitor of myosin ATPase, perturbs coiling morphogenesis of the isolated gut explants *in vitro*.
(B-E) Blebbistatin inhibited the gut coiling morphogenesis in a concentration-dependent manner, and so reduced the probability of successful looping after 1 day of culture (E), suggesting that actomyosin interaction-mediated contraction is essential for the gut looping. Control explant culture was performed using siblings (A), showing high incidence of successful looping. Scale bars = 500 μm.

Figure 13
Y-27632, an inhibitor of ROCK (Rho-associated coiled-coil-containing protein kinase, Rho kinase), strongly arrests coiling morphogenesis of the isolated gut explants.
(A' and C) Y-27632 completely stopped the coiling of the isolated gut after 1 day of culture (C). (B and B') Immunostaining of SM-actin revealed that Y-27632 inhibited the polymerization of SM-actin filaments (B'). Control experiments were performed using siblings (A and B). Scale Bars are 500 μm for A and A', 100 μm for B and B'.

Figure 14
Wnt C-59, an inhibitor of Wnt signaling pathway, prevents coiling morphogenesis in isolated gut explants.
(B-D, G) Wnt C-59 decreased the incidence of successful looping of the isolated gut after 1 day of culture (G). (E and F) Immunostaining of SM-actin demonstrating that Wnt C-59 inhibited the polymerization of SM-actin filaments (F). Control experiments were performed using siblings (A and E). Scale Bars are 500 μm for A–D, 100 μm for E and F.

Figure 15
Administration of Cardionogen-1 (Wnt canonical pathway inhibitor) inhibits gut coiling morphogenesis.
(A-D) After the cardionogen-1 treatment by 2 days of incubation until control siblings reached stage

46, gut coiling morphogenesis was perturbed, and in numerous cases, only the dorso-ventral meander of the gut was observed (B and D). (E and F) Immunostaining of SM-actin revealed that Cardionogen-1 disordered the organization of smooth muscle cellular meshwork and its torsion (F). Scale Bars are 500 μm for A and B, 1 mm for C and D, 50 μm for E and F.

Table 1

Effects of (±)-Blebbistatin treatment on larval organ morphology.

After 6 h of (±)-Blebbistatin treatment at 24°C from stage 38–39 to stage 39–40, coiling of the intestinal tube is perturbed, with cancellation of left-right asymmetry in numerous cases (Fig. 4).

Table 2

Effects of each Blebbistatin optical isomer.

S-(–)-Blebbistatin has significant effects on gut coiling morphogenesis, similar to (±)-Blebbistatin, while R-(+)-Blebbistatin has no effect (Fig. 5). Thus, S-(–)-Blebbistatin is the active isomer of (±)-Blebbistatin in *Xenopus* larvae, as demonstrated previously for mammals.

Table 3

Evaluation of the extent of gut coiling after decapitation and amputation of the heart and/or tail.

After performing decapitation and amputation at stage 32–33 (tailbud stage), as shown in Fig. 7A, partial embryos were reared to become larvae, and the extent of gut looping was scored when normal siblings reached stage 46.

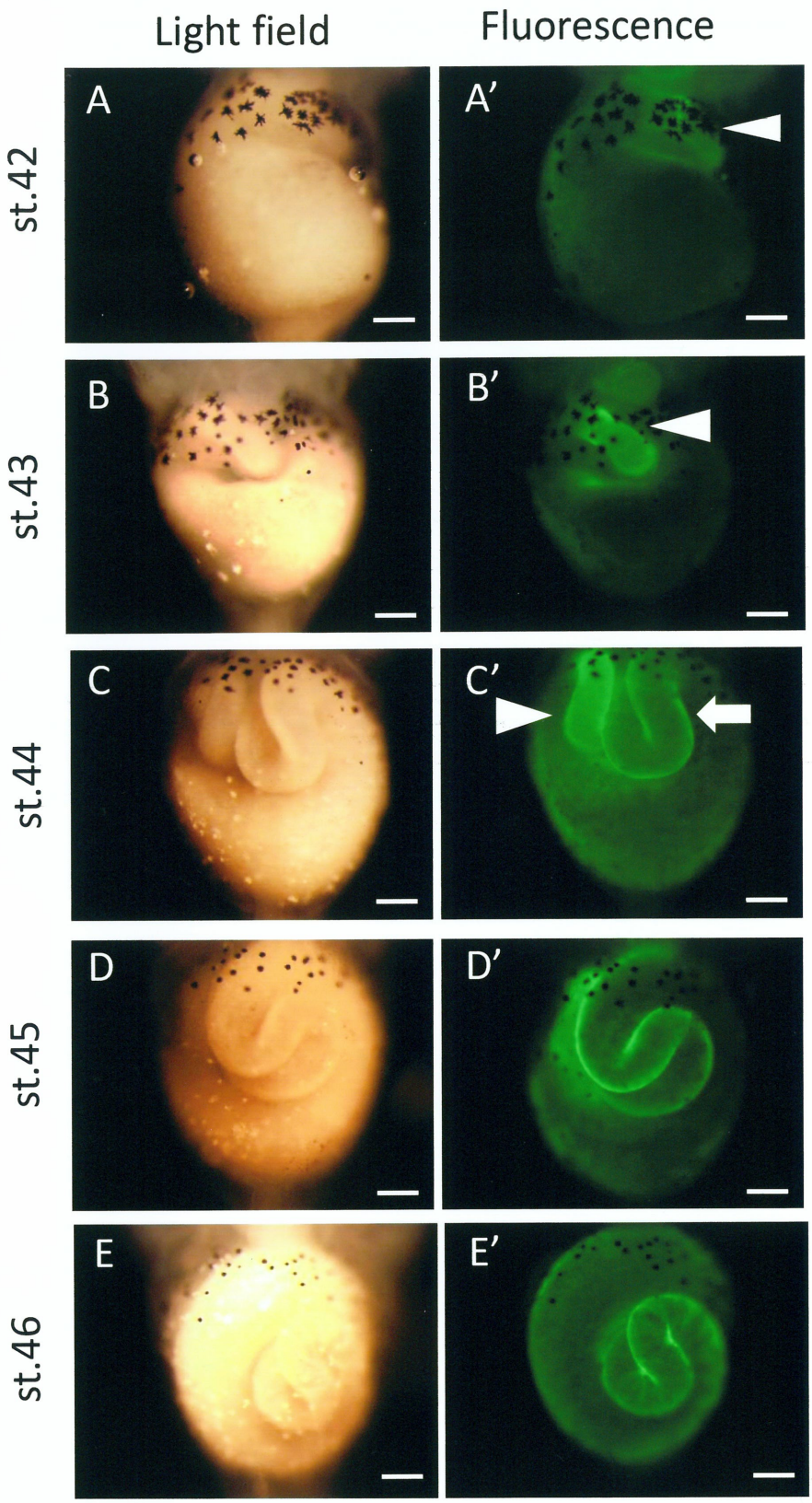
Light field
Fluorescence
st.42
st.43
st.44
st.45
st.46
A
A'
B
B'
C
C'
D
D'
E
E'

Fig. 1

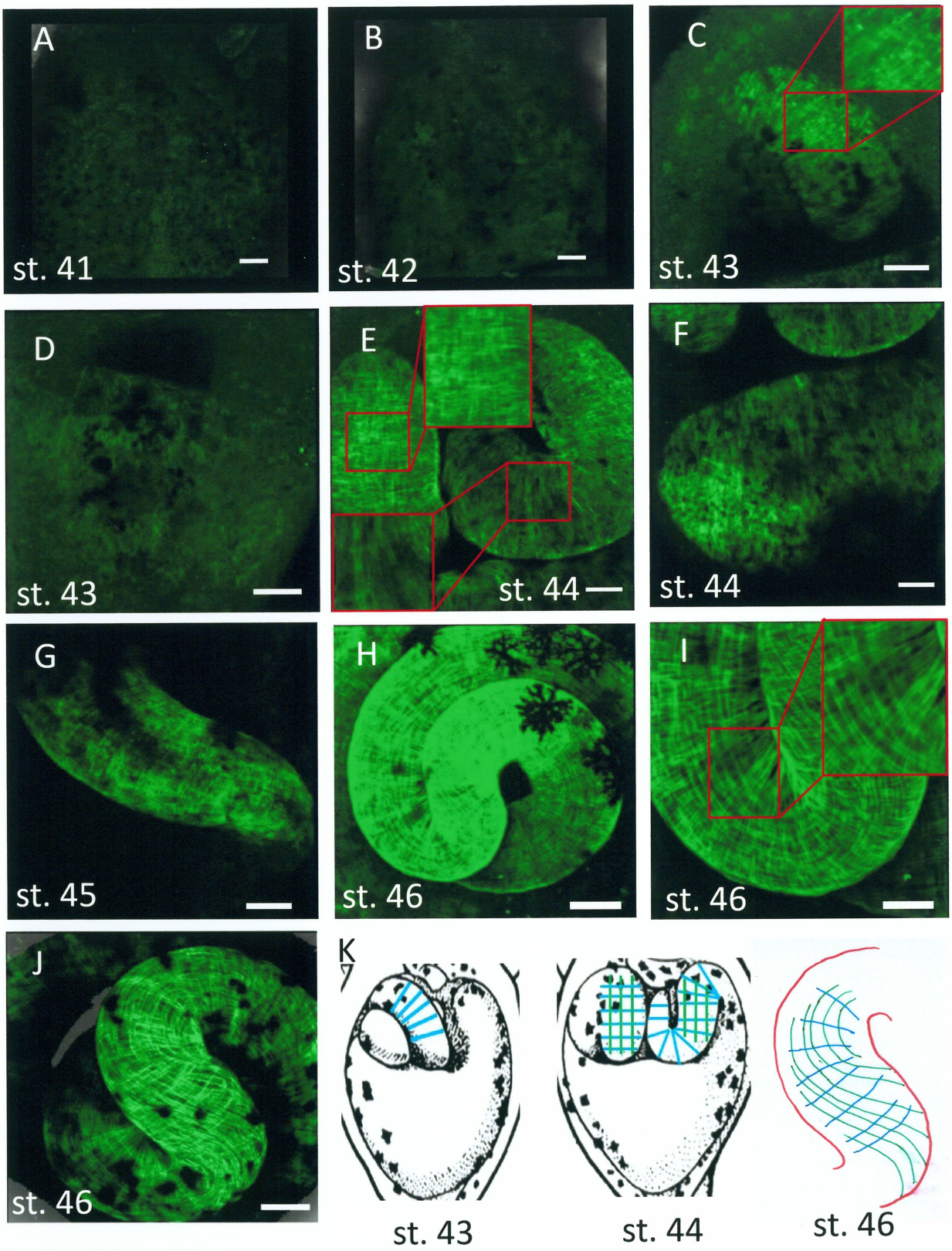
A
st. 41
B
st. 42
C
st. 43
D
st. 43
E
st. 44
F
st. 44
G
st. 45
H
st. 46
I
st. 46
J
st. 46
K
st. 43
st. 44
st. 46

Fig. 2

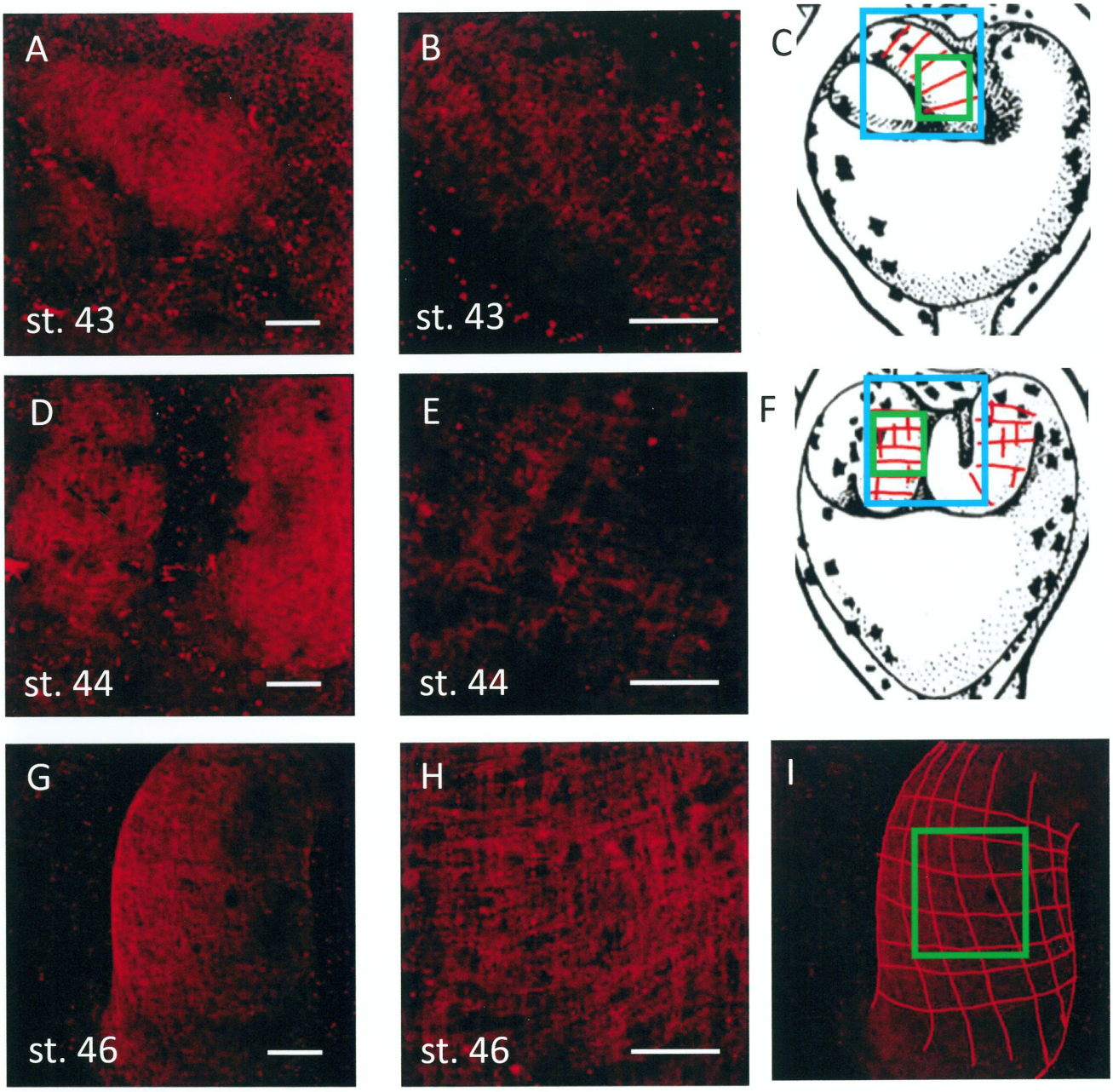

Fig.3

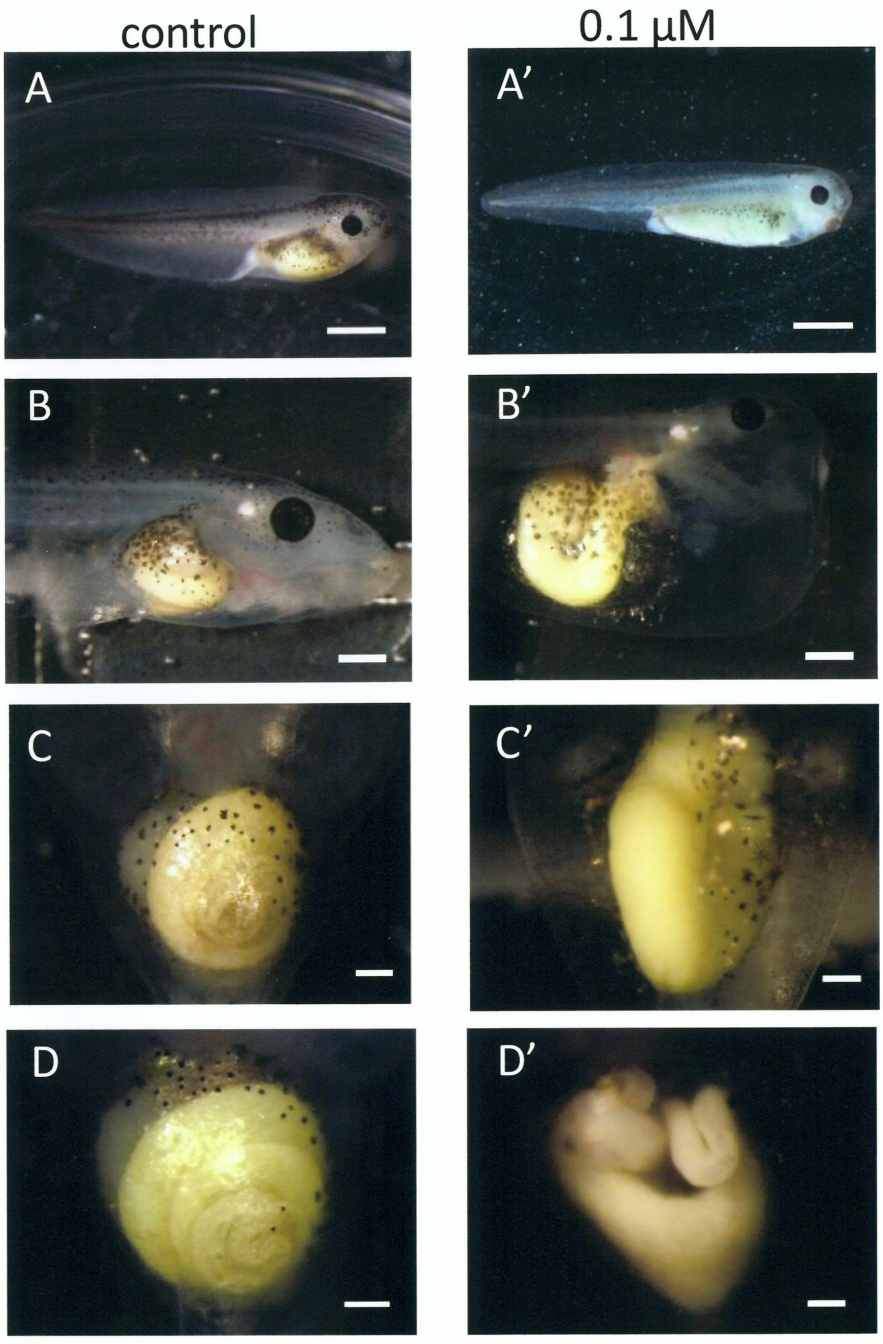

Fig. 4

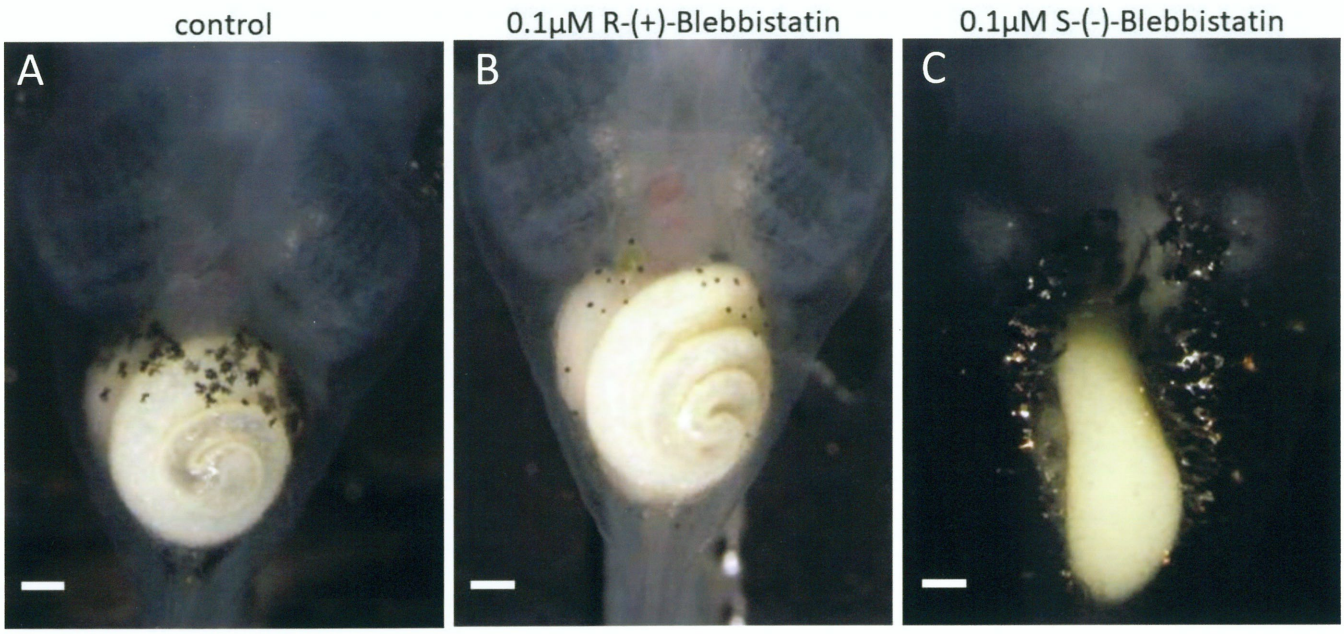

Fig. 5

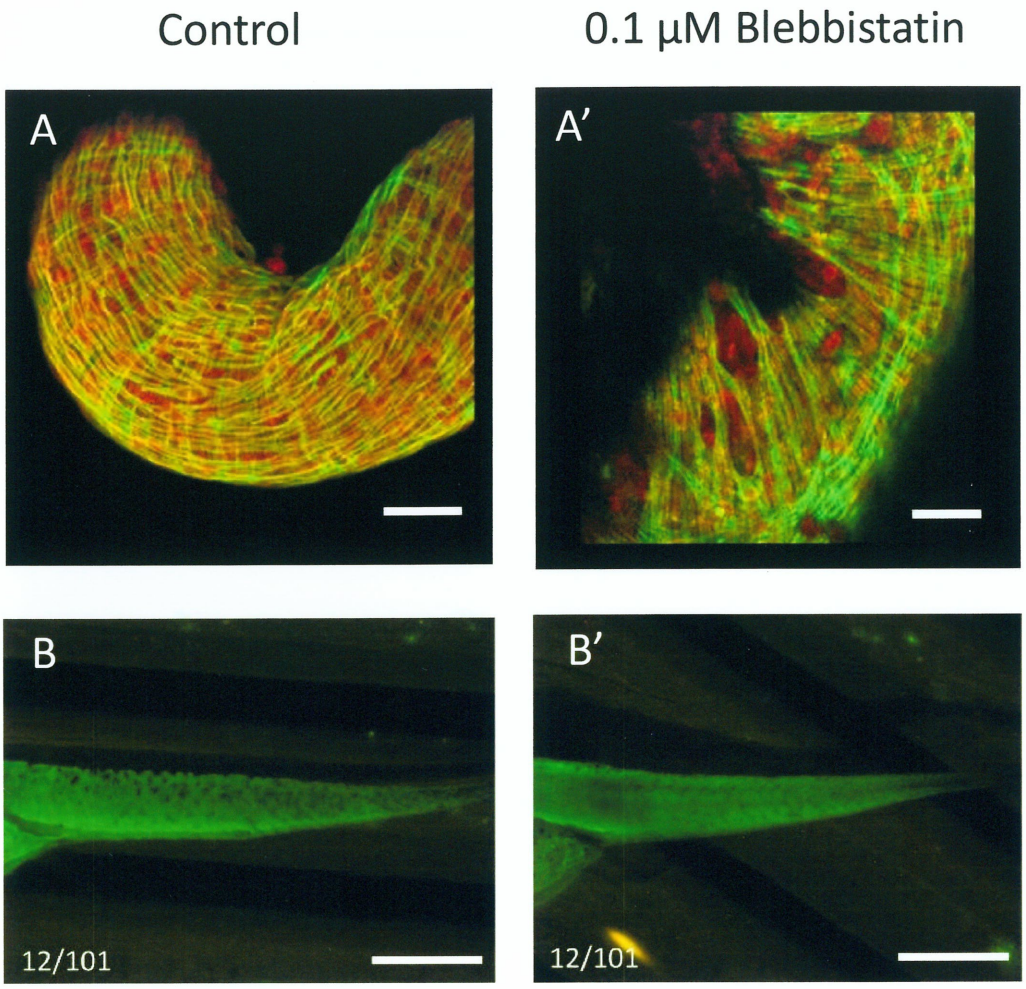

Fig.6

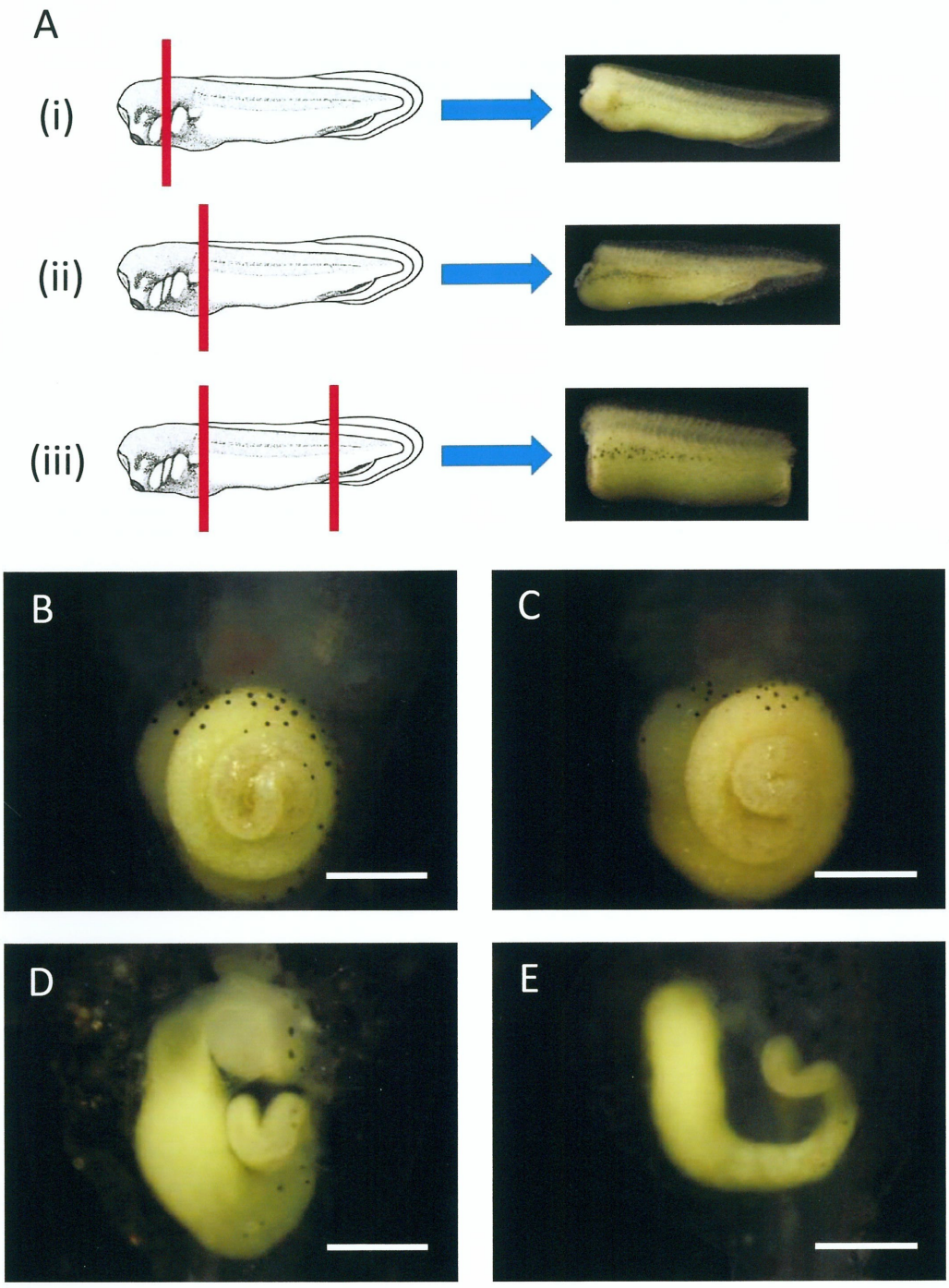

Fig.7

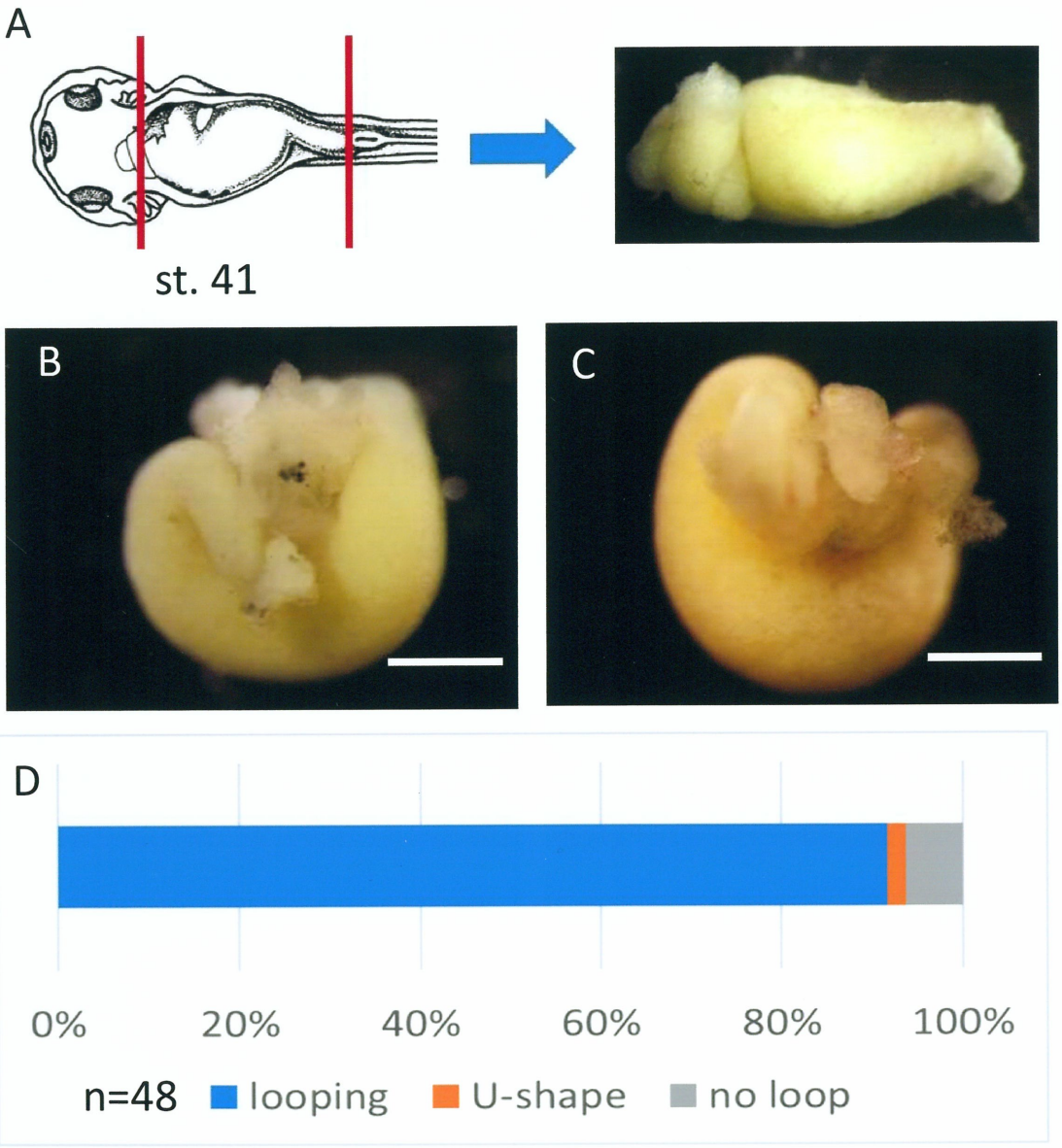

Fig. 8

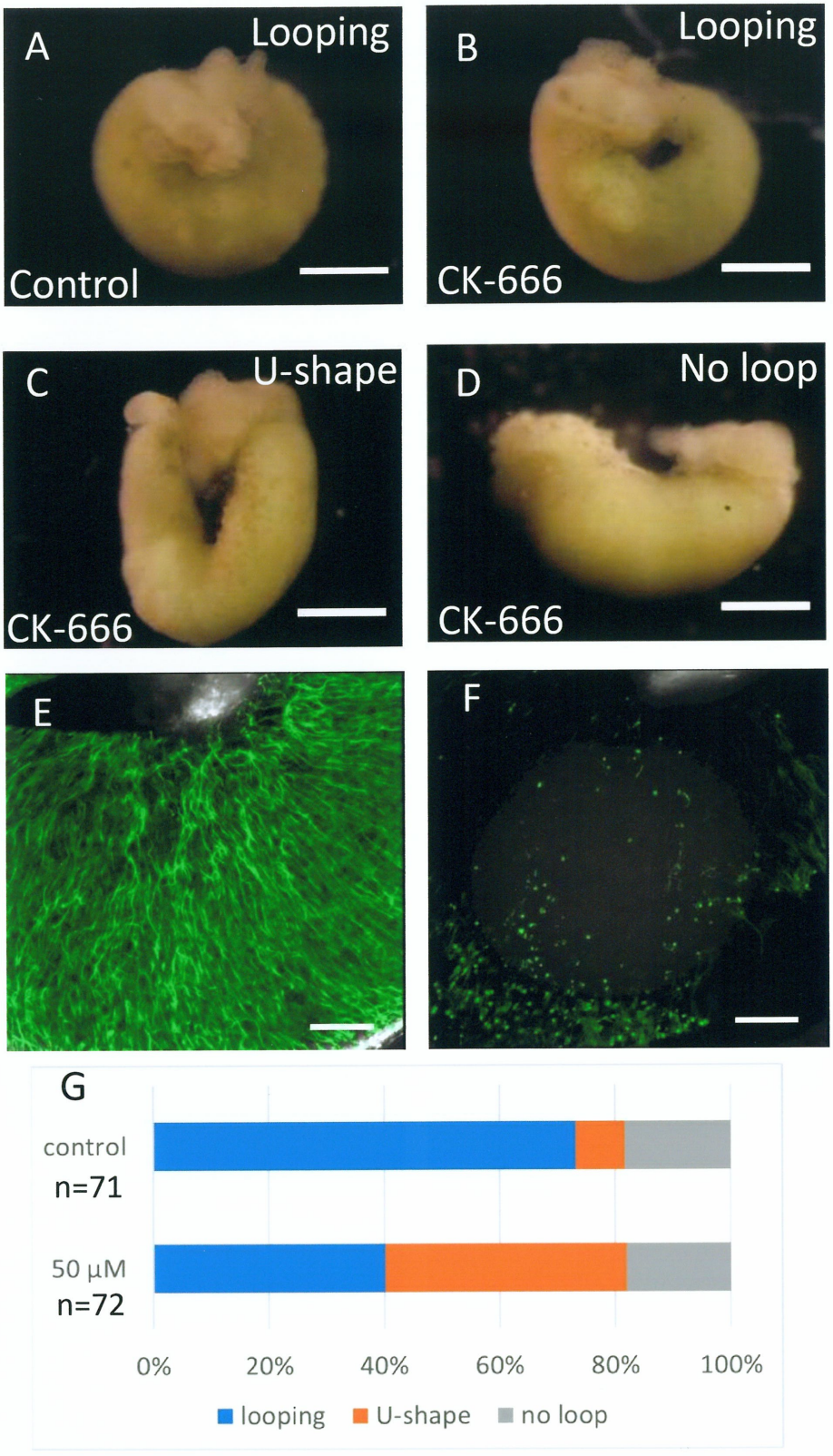
A
Looping
Control
B
Looping
CK-666
C
U-shape
CK-666
D
No loop
CK-666
E
F
G
control
n=71
50 µM
n=72
0%
20%
40%
60%
80%
100%
looping
U-shape
no loop

Fig. 9

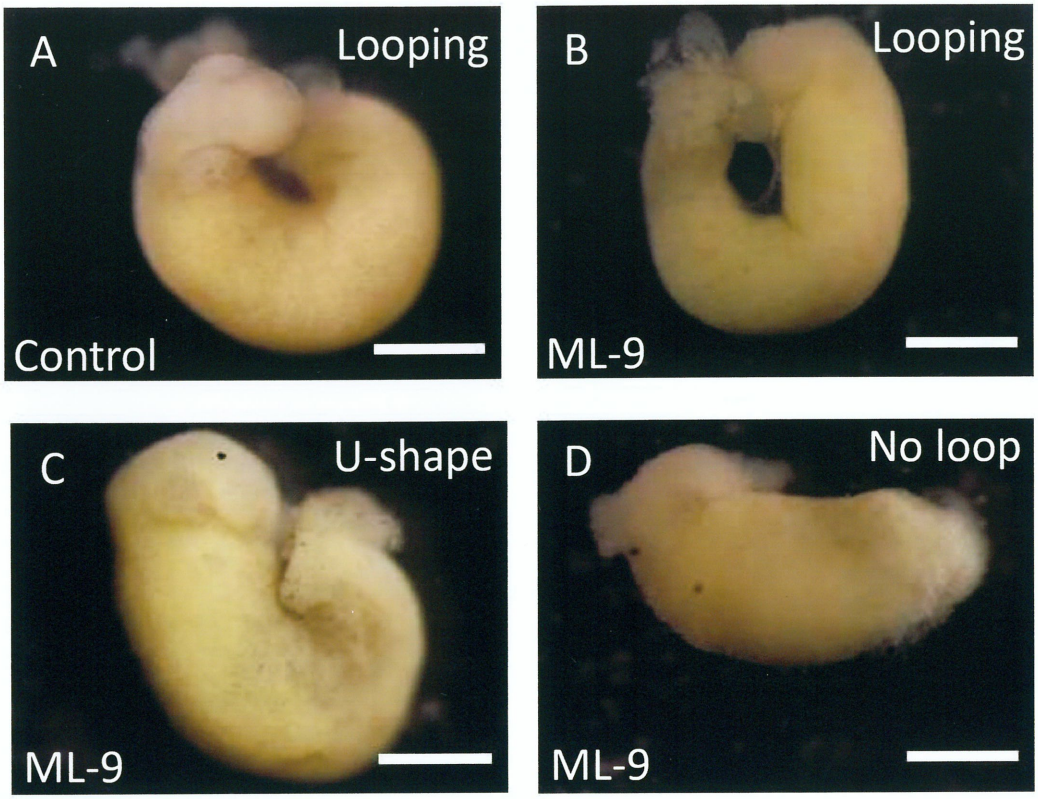
A
Looping
Control
B
Looping
ML-9
C
U-shape
ML-9
D
No loop
ML-9

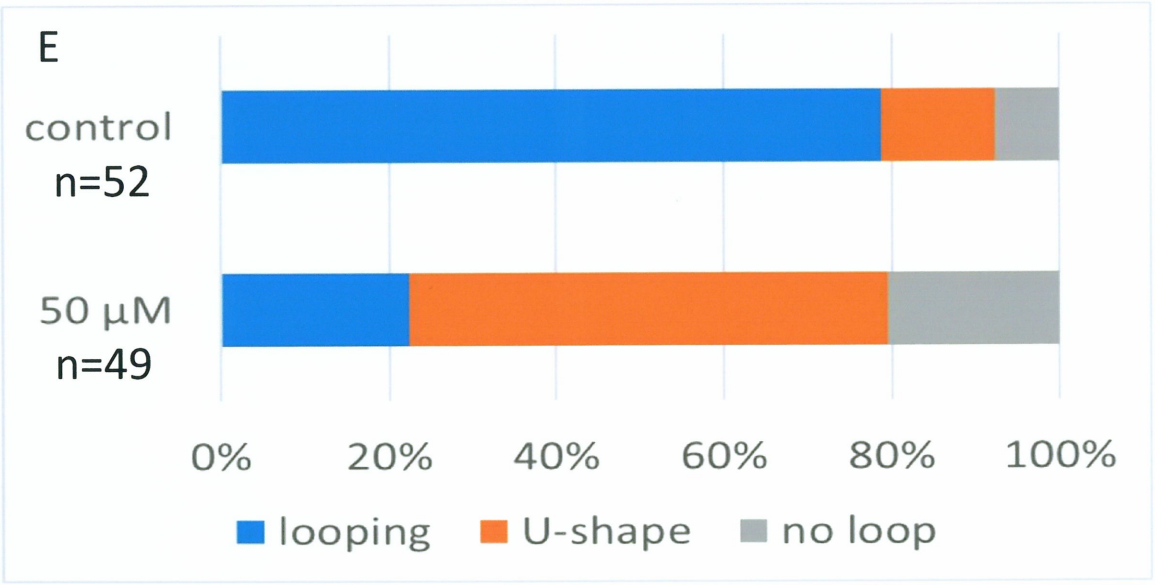
E
control
n=52
50 µM
n=49
0%
20%
40%
60%
80%
100%
looping
U-shape
no loop

Fig. 10

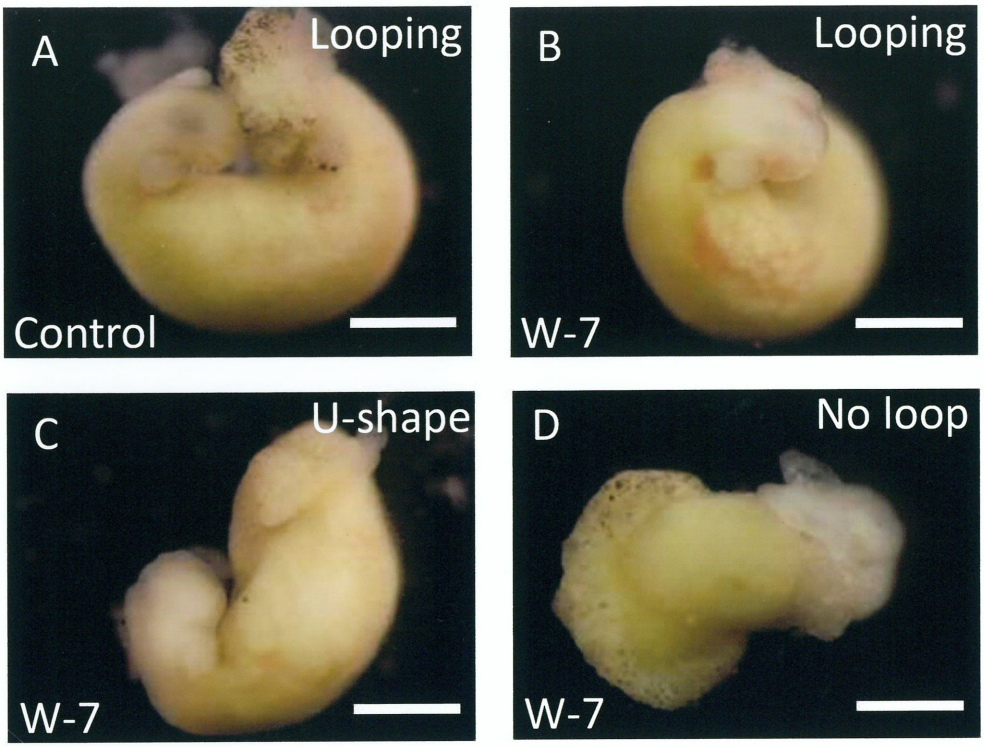
A
Looping
Control
B
Looping
W-7
C
U-shape
W-7
D
No loop
W-7

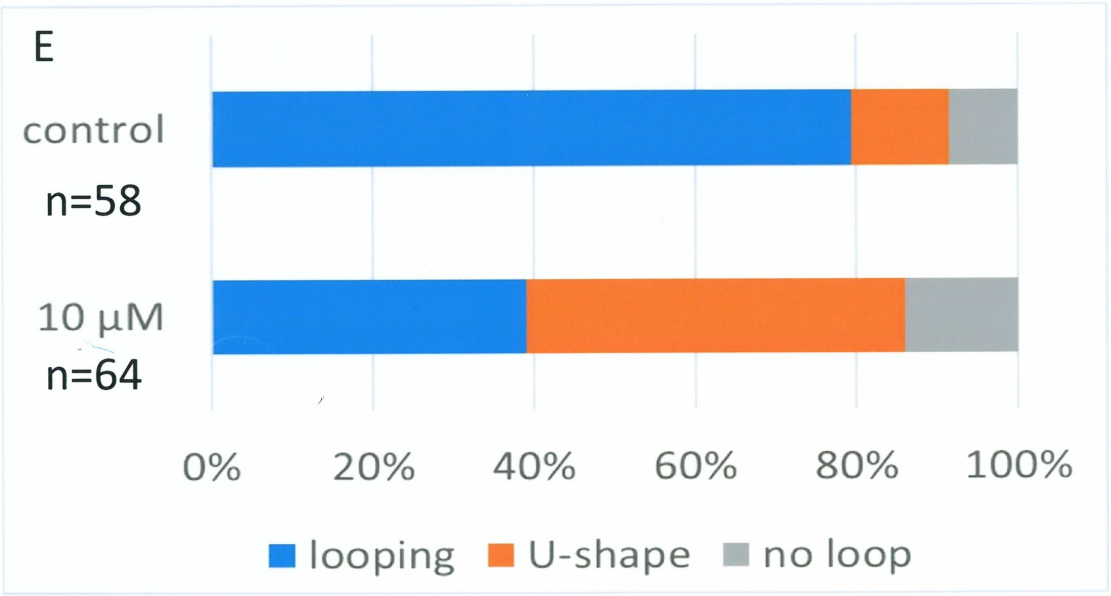
E
control
n=58
10 µM
n=64
0%
20%
40%
60%
80%
100%
looping
U-shape
no loop

Fig. 11

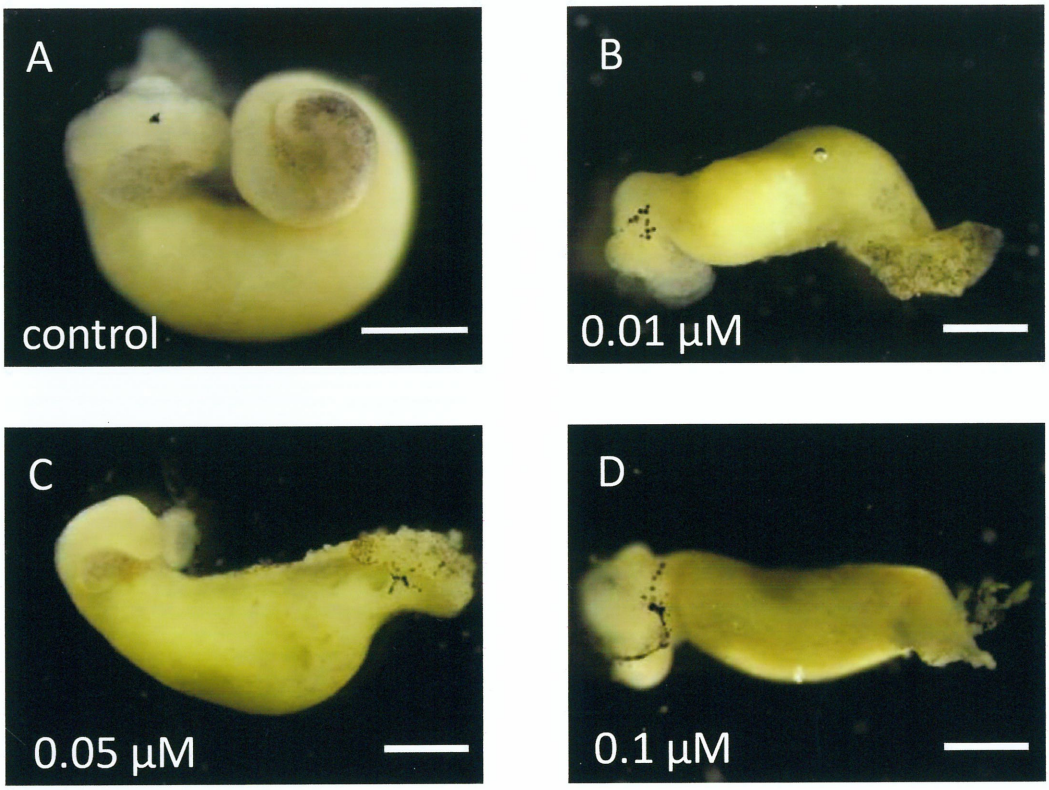
A
control
B
0.01 µM
C
0.05 µM
D
0.1 µM

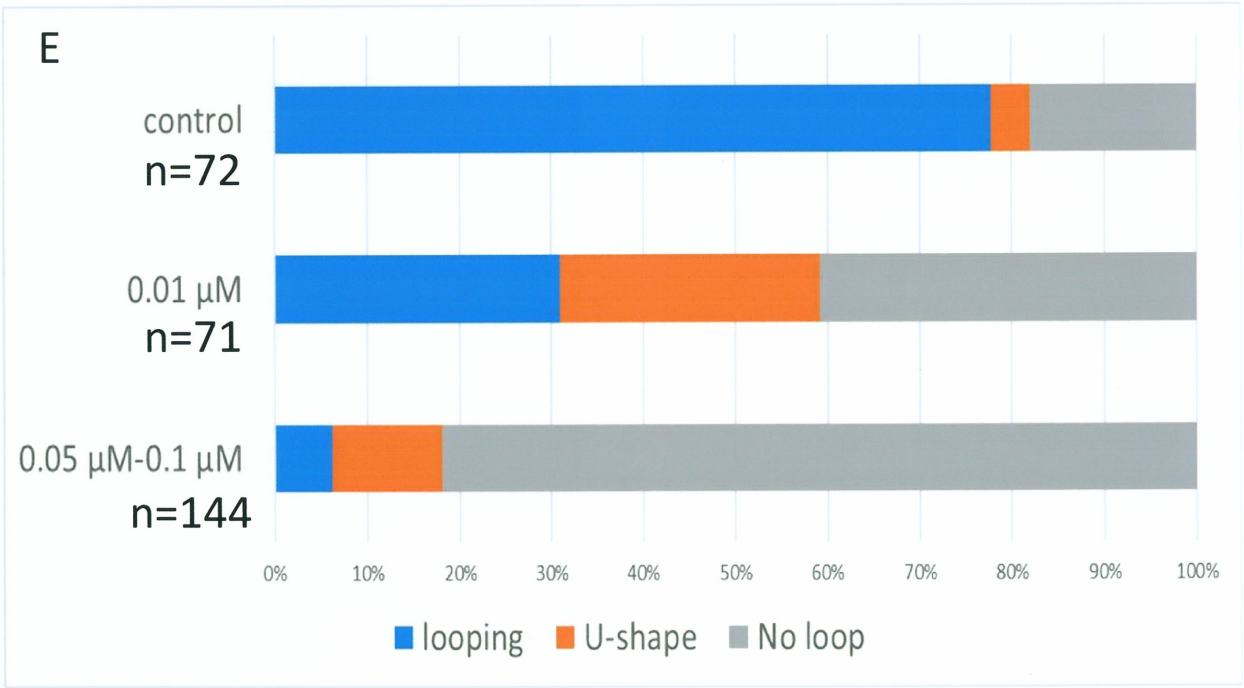
E
control
n=72
0.01 µM
n=71
0.05 µM-0.1 µM
n=144
0%
10%
20%
30%
40%
50%
60%
70%
80%
90%
100%
looping
U-shape
No loop

Fig.12

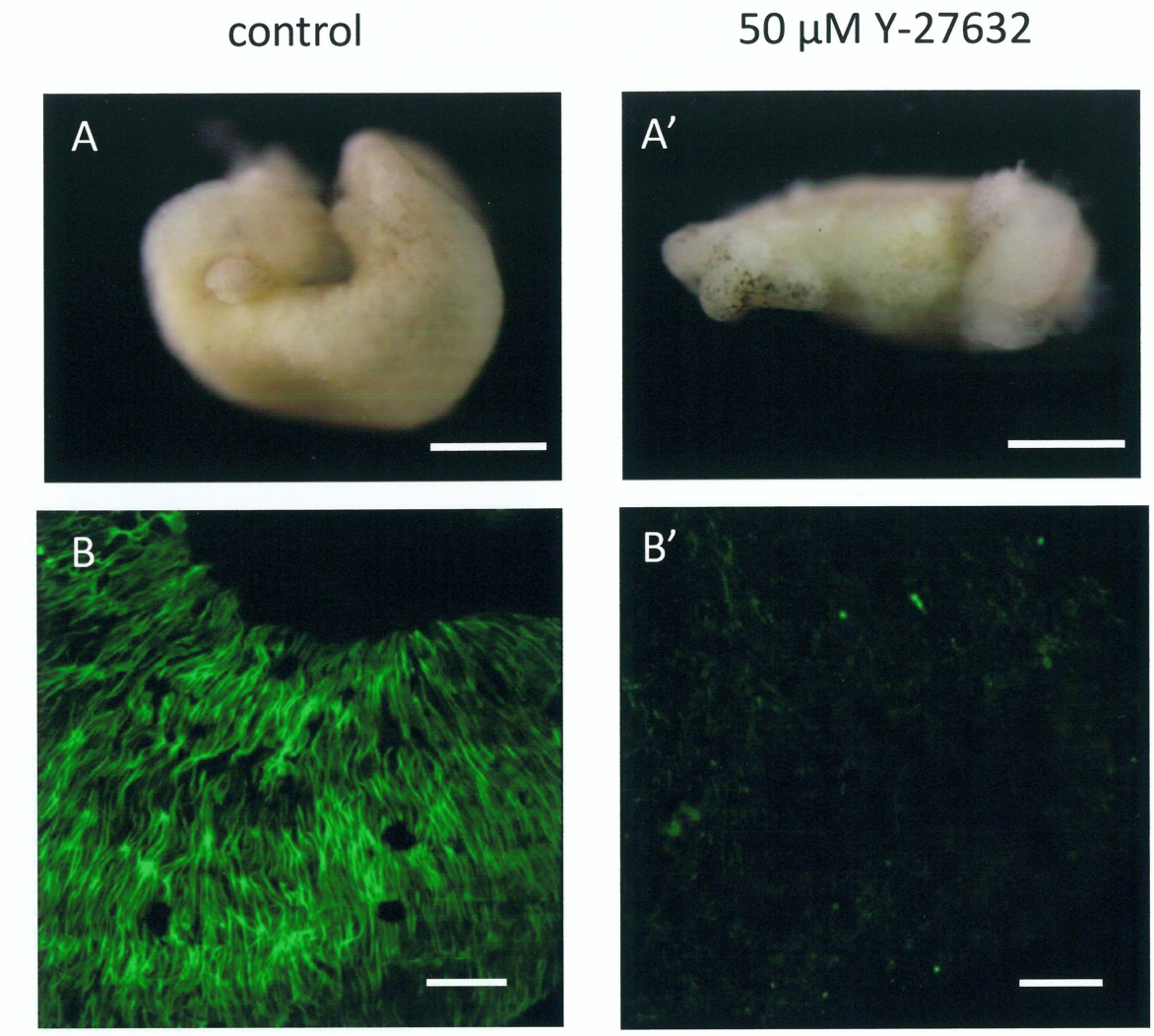
control
50 μM Y-27632
A
A'
B
B'
C
control
n=60
50 μM
n=57
0%
20%
40%
60%
80%
100%
looping
U-shape
no loop

Fig.13

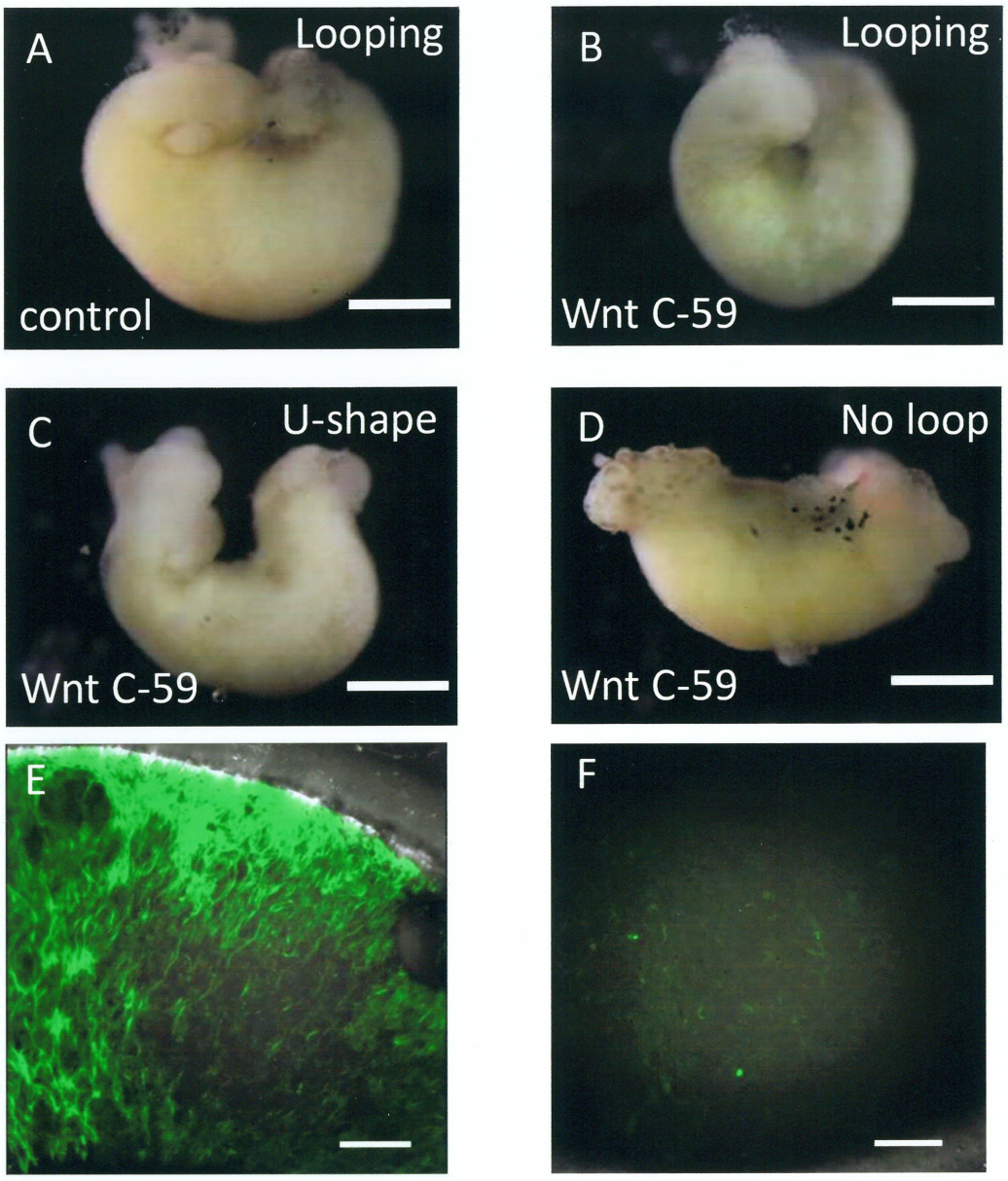
A
Looping
control
B
Looping
Wnt C-59
C
U-shape
Wnt C-59
D
No loop
Wnt C-59
E
F

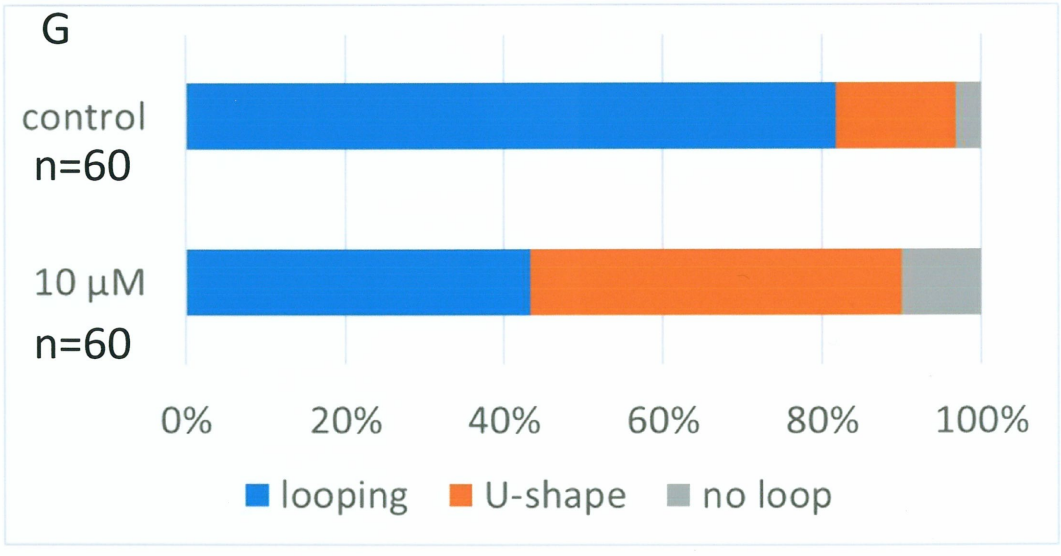
G
control
n=60
10 µM
n=60
0%
20%
40%
60%
80%
100%
looping
U-shape
no loop

Fig.14

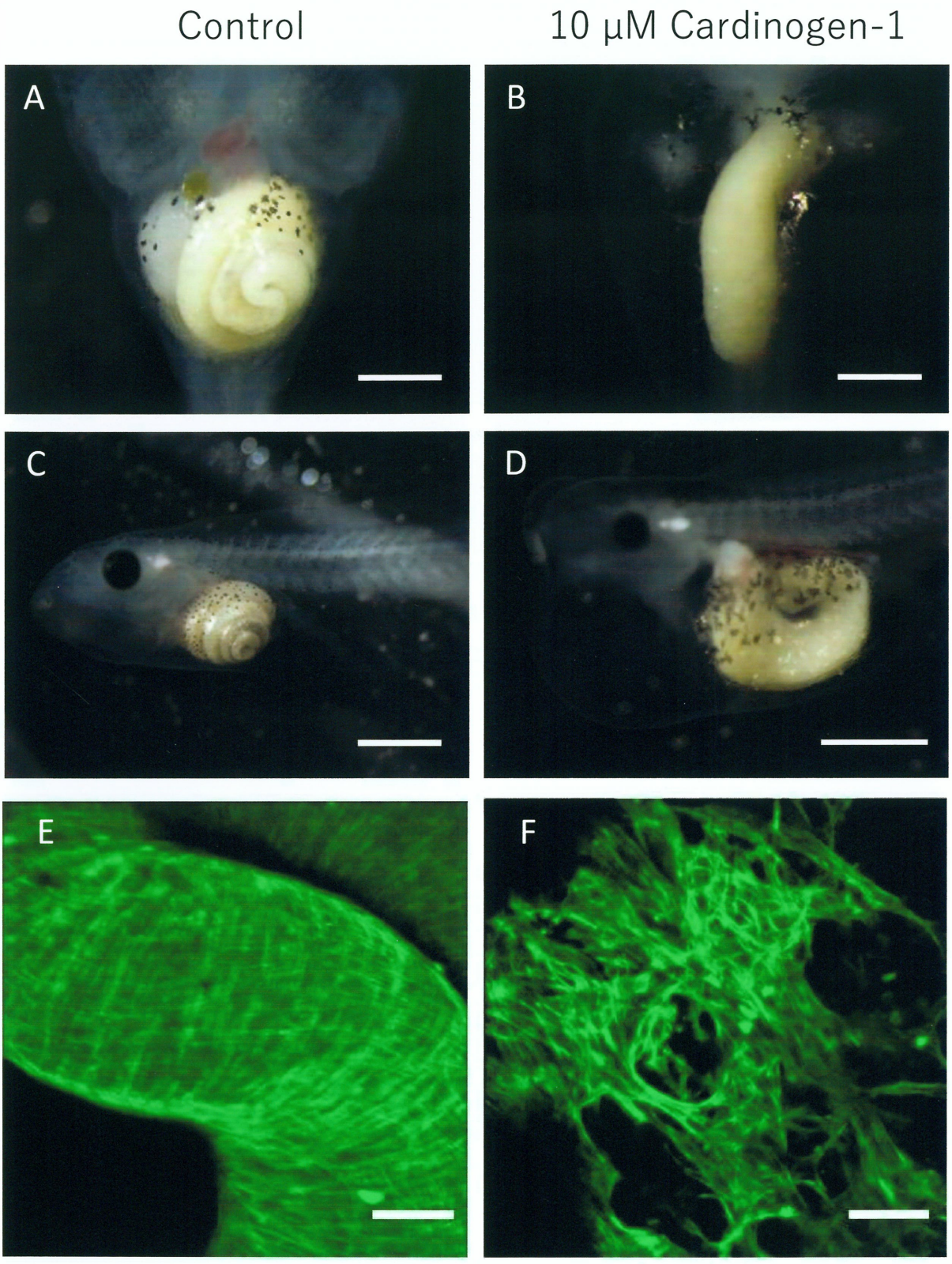

Fig.15

Table 1

	Number of samples	Survived (survival ratio; %)	Inhibition of gut looping	Cancellation of L–R asymmetry
control	60	60 (100)	4	0
0.05 μM	60	45 (75)	27	18
0.1μM	60	51 (85)	29	22

Effects of (±)-Blebbistatin treatment on larval organ morphology

After 6 h of (±)-Blebbistatin treatment at 24°C from stage 38–39 to stage 39–40, coiling of the intestinal tube is perturbed, with cancellation of left-right asymmetry in many cases (Fig. 4).

Table 2

		Number of samples	Survived (survival ratio; %)	Inhibition of gut looping	Cancellation of L-R asymmetry
	control	36	36 (100)	1	0
R-(+)	0.05 μM	36	36 (100)	0	0
	0.1 μM	36	36 (100)	1	0
S-(-)	0.05 μM	36	19 (52.7)	10	9
	0.1 μM	36	29 (80.5)	21	8

Effects of each Blebbistatin optical isomer

S-(–)-Blebbistatin has significant effects on gut looping morphogenesis, similar to (±)-Blebbistatin, while R-(+)-Blebbistatin has no effect (Fig. 5). Thus, S-(–)-Blebbistatin is the active isomer of (±)-Blebbistatin in Xenopus larvae, as demonstrated previously for mammals.

Table 3

	Number of samples	Number of the survived	Normal gut looping	Inhibition of gut looping	Edema
control	72	72	72	0	0
decapitation with heart	70	70	69	1	4
decapitation without heart	71	71	15	56	71
torso-like (*)	35	35	4	31	35

*...decapitation without heart and tail

Evaluation of the extent of gut looping after decapitation and amputation of the heart and/or tail.
After performing decapitation and amputation at stage 32–33 (tailbud stage), as shown in Fig. 7A, partial embryos were reared to become larvae, and the extent of gut looping was scored when normal siblings reached stage 46.